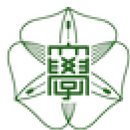
HOKKAIDO UNIVERSITY

Title	Temperature Dependence of Electric Field Control of Electron Spin Polarization in Semiconductor Quantum Well-Dot Coupled Nanostructures
Author(s)	朴, 昭暎
Citation	北海道大学. 博士(工学) 甲第15543号
Issue Date	2023-03-23
DOI	10.14943/doctoral.k15543
Doc URL	http://hdl.handle.net/2115/89816
Type	theses (doctoral)
File Information	Soyoung_Park.pdf

Instructions for use

Hokkaido University Collection of Scholarly and Academic Papers : HUSCAP

令和 4 年度

Doctoral Dissertation
博士学位論文

Temperature Dependence of Electric Field Control of Electron Spin Polarization in Semiconductor Quantum Well-Dot Coupled Nanostructures

半導体量子井戸-ドット結合ナノ構造における電子スピン偏極の電界制御の温度依存性

Graduate School of Information Science and Technology

Hokkaido University

北海道大学大学院情報科学院

Soyoung Park

朴 昭暎

Acknowledgements

First and foremost, I would like to express my deepest gratitude to my advisor Prof. Akihiro Murayama for all the guidance, support, and feedback of my study. His guidance and immense knowledge helped me in all the time of research and writing of this thesis. I was able to learn the research mindset and attitude thanks to his encouragements.

I would also like to extend my sincere thanks to my thesis committee: Prof. Junichi Motohisa and Prof. Kazuhisa Sueoka, for their suggestion and insightful comments to revise my thesis.

I wish to thank Prof. Kazuhisa Sueoka and Associate Prof. Agus Subagyo in the Laboratory of Nanoelectronics for their supports in fabricating my devices.

I am also grateful to Associate Prof. Satoshi Hiura and Mr. Junichi Takayama for their insightful comments, suggestions, and technical support on my study. Furthermore, I would like to thank all the members in the Laboratory of Electronic and Photonic Materials for their kind help and support that have made my study and life in Japan. I think I was very lucky to study in this laboratory.

I would like to thank my family: my parents and to my brother for supporting me spiritually and encouraging me not to give up.

Finally, I am grateful to the financial support provided by the Japanese Government (MEXT) Scholarship Programs for Research students (2018.04-2023.03).

Contents

Acknowledgements 1
Chapter 1. Introduction 4
1.1 Background 4
1.2 History of spintronics 5
1.3 Electron spin 13
1.4 Generation of electron spin 15
1.5 Relaxation of electron spin 18
1.5.1 D'yakonov-Perel' mechanism 18
1.5.2 Elliott-Yafet mechanism 20
1.5.3 Bir-Aronov-Pikus mechanism 21
1.5.4 Spin-orbit interaction 22
1.6 Semiconductor quantum dot 25
Bibliography 28
Chapter 2. Research purpose 32
2.1 Background 32
2.1.1 Spin injection in QW/QD tunnel-coupled nanostructures 32
2.1.2 Spin manipulation using electric field 34
2.1.3 Spin flip scattering 36
2.2 Research purpose 38
Bibliography 40
Chapter 3. Experimental Procedures 41
3.1 Device fabrication 41
3.2 Circularly polarized photoluminescence measurement 42
Chapter 4. Temperature dependence of spin polarization with electric field in InGaAs QW/QD coupled structure 44
4.1 Background 45
4.2 Experimental procedures 45
4.3 Bias dependence of electron-spin polarization at 4 K 47
4.4 Temperature dependence of electron-spin polarization 51
4.5 Electric-field control of electron-spin polarization at RT 55
4.6 Conclusion 62
Bibliography 63

Chapter 5. Electric-field-effect on spin polarization in InGaAs QW/InAs QD coupled structure 64
5.1 Background 64
5.2 Experimental procedures 64
5.3 Bias dependence of electron-spin polarization at 4 K 65
5.4 Temperature dependence of electron-spin polarization 68
5.5 Bias dependence of electron-spin polarization at RT 70
5.6 Conclusion 71
Bibliography 72
Chapter 6. Electric-field-effect on spin polarization in GaNAs QW/InAs QD 73
6.1 Background 73
6.2 Experimental procedures 74
6.3 Bias dependence of electron-spin polarization at RT 75
6.4 Conclusion 80
Bibliography 80
Chapter 7. Conclusion 82
Research achievements 84
Publications 84
Conferences 85

Chapter 1. Introduction

1.1 Background

For traditional information processing, semiconductor devices are generally performed by controlling electron charges, which can be positive or negative. However, as the size of the semiconductor devices decreases to several nanometer scales by using the advanced microfabrication process, it brings three main issues. First, the distance between the electron source and drain which called a channel in semiconductor devices becomes narrow. This short-channel effect results in the threshold-voltage reduction, a hot carrier effect, direct source-drain tunneling and so on [1, 2]. Especially, direct electron tunneling makes it difficult to control electric current in circuits. Second, the high integration density of transistor on a small chip generates heat. Finally, the smaller chip size makes the higher manufacturing cost because of increasing costs for designing chip and lithography systems [3]. Furthermore, it has been predicted that the limit of Moore's law, regarding as a key index of semiconductor manufacturing, can be reached soon [4], or already it may be ended. Thus, development of new technology that exceeds the limit of these problems has strongly been required for future information processing systems.

Semiconductor spintronics was introduced with superior device characteristics such as low power consumption, using both electron charges and spin angular momenta of electrons [5]. In addition, the limitation of Moore's Law is probably not a big problem for the spintronics because the electron spin itself has the polarization as an information carrier. Therefore, it is expected that the spintronics will contribute greatly to the development of memory application and information processing without enormous electric power consumption. The electrons have two spin directions (i.e., polarizations) of up- and

down state, which are defined as different momenta with the spin quantum number of +1/2 and −1/2, respectively. These two momenta of electron spin can be substituted to the binary number system of 1 and 0, for example. However, the electron-spin polarization is significantly randomized during transport by some interaction and scattering mechanisms in layered semiconductor device structures, particularly at room temperature (RT), and it is so-called spin relaxation. Therefore, to realize practical spintronic devices using semiconductor materials, the spin-polarized electron must be detected at RT with maintaining its spin-state without the marked relaxation during transport [6].

Recently, opto-spintronics field is an innovative application of semiconductor spintronics because optical wiring technology can reduce power consumption and transmission losses. Semiconductor quantum dots (QDs) have been studied as a promising device material for optically active layers of opto-spintronic devices. Three-dimensional (3D) strong quantum confinements in the QDs lead to the suppressed spin relaxation as well as superior optical properties with discrete energy level separation.

1.2 History of spintronics

Spintronics began to attract attention with the development of thin film technology and fabrication of nanostructures. A flow of spin angular momentum, called as spin-current, markedly decreases with a spin-diffusion length of ~1 μm, and this is not appropriate for traditional electric devices due to insufficient spin current manipulation. However, the spin current becomes play an important role for nanostructures as decreasing the size of chip, and then the spin current can be controlled in spintronic devices. Spintronics is largely divided into two fields: spintronics in metal and semiconductor. Figure 1-1 indicates a brief

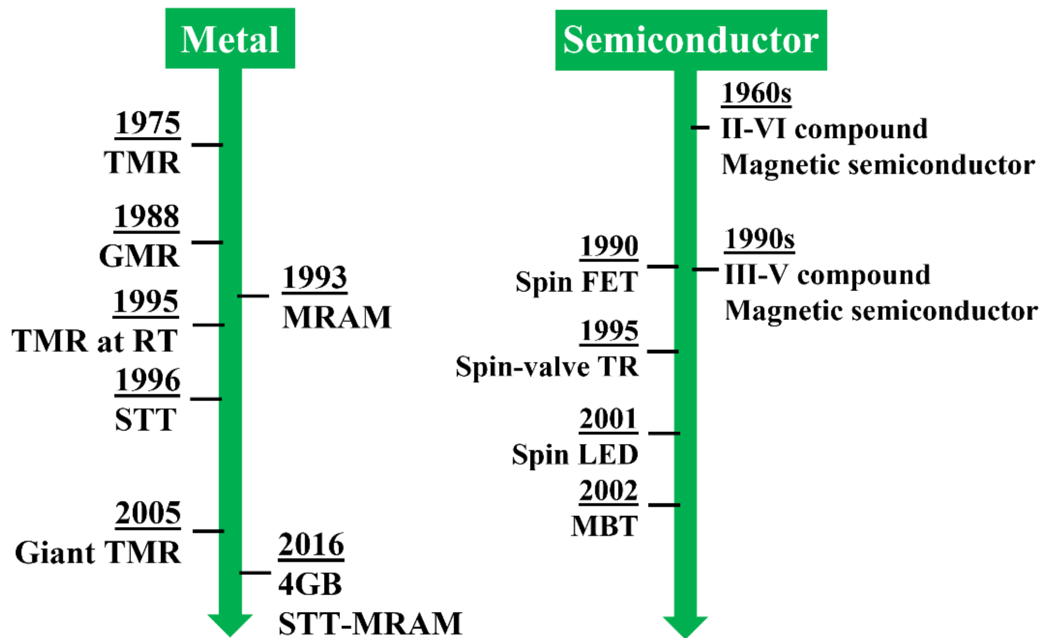

Figure 1-1 History of spintronics: metal (left) and semiconductor (right) spintronics.

history of these spintronics. Initial spintronics has been originated from a magnetoresistance (MR) effect, which is that an electric-resistance changes depending on the applied magnetic field in a metallic ferromagnetic (FM)/non-magnetic/FM stacking layer. A ratio of magnetic-field-induced resistance change to the basic resistance is called as MR ratio, which is essential for sensitivity of a magnetic-field sensor. The tunnel magnetoresistance (TMR) was found by reducing a thickness of non-magnetic tunneling layer in 1975 [7, 8], and this TMR is currently playing an important role to produce hard-disk drives. In 1988, the giant magnetoresistance (GMR) was discovered, and it led to the TMR effect at RT in 1995, which contributes to the development of ultrasensitive magnetic-field sensors for biomedical applications [9, 10, 11]. Figure1-2 (a) and (b) show schematic plots of the GMR structure and their resistance changes depending on the magnetization. If the spin orientation of an injected electron is parallel to the magnetization of ferromagnetic material (Fig.1-2a), the resistance is small. However, in anti-parallel case (Fig.1-2b), high electrical resistance is obtained in the ferromagnet due to the strong spin-dependent scattering. The MR ratio

of the GMR is obtained with two resistances R_p and R_{ap}, following an equation:

$$\text{MR ratio} = \frac{(R_{ap} - R_p)}{R_p} \times 100. \quad (1\text{-}1)$$

Here, R_p and R_{ap} are resistances of the layers when spin orientation and magnetization is parallel and anti-parallel, respectively. In short, GMR is defined by the spin-dependent scattering, and it results in the difference of electrical conduction depending on the magnetization of ferromagnetic materials controlled by an external magnetic field. On the other hand, a spin-dependent tunneling is important for the TMR. Figure 1-2 (c) and (d) show schematic plots of Julliere's model accounting for a principle of the TMR [7]. It is assumed that the spin angular momentum

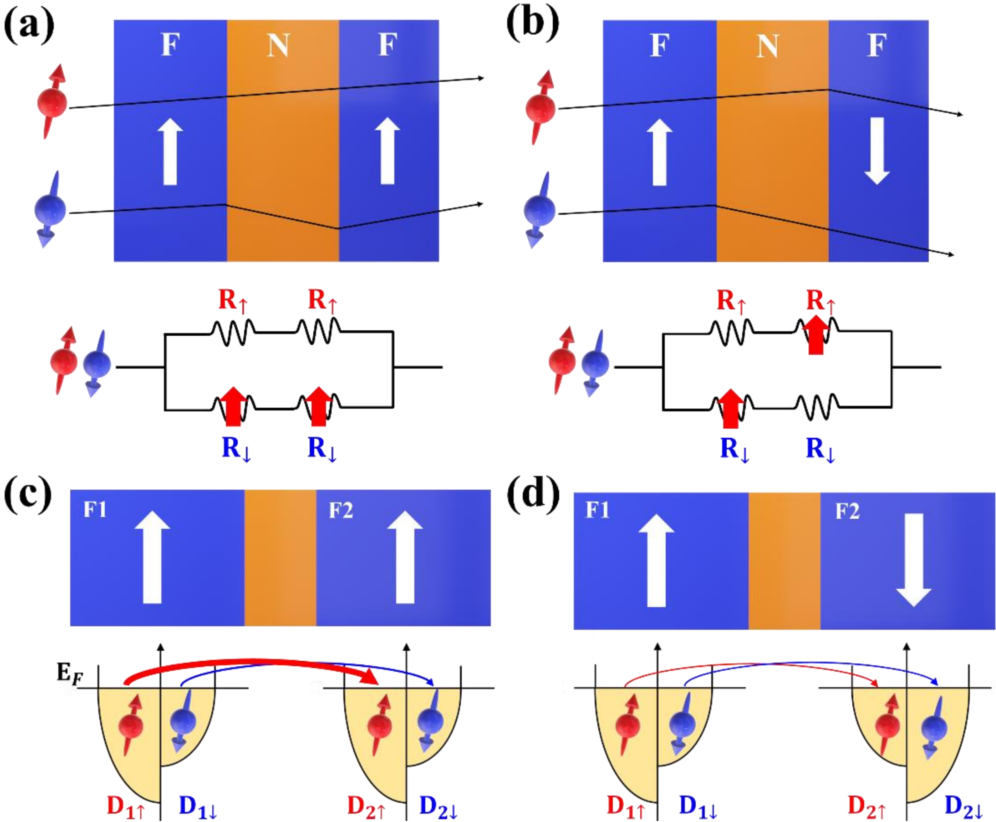

Figure 1-2 Schematic plots of GMR and TMR effect and diagrams of their principles. F and N mean ferromagnetic and non-magnetic materials, respectively. The magnetization directions between the two ferromagnetic layers are parallel (a, c) or anti-parallel (b, d). If the spin orientation of a conduction electron is anti-parallel to the magnetization direction, a resistance of the layer is higher than the parallel case.

is conserved during tunneling. Similar to the above GMR, the tunneling current can flow easily from ferromagnet F1 to F2 due to its small resistance when the magnetization between two different ferromagnetic materials is parallel each other. The MR ratio of this TMR (~300 %) is normally bigger than that of the GMR (~65 %) at RT [12] and the ratio strongly depends on the electron-spin polarization P of the ferromagnetic materials with a following equation [7]:

$$MR = \frac{2P_1P_2}{1 - P_1P_2} \quad (1\text{-}2)$$

To increase this MR ratio, half-metal materials like CrO_2 or $La_xSr_{1-x}MNO_3$ have recently received attention due to the spin polarization of 100 % at the Fermi energy (E_F). Furthermore, a magnetic tunnel junction (MTJ) using a MgO tunneling barrier has been studied, and the giant TMR with large MR ratios up to 180 % at RT was observed in 2004 [13].

Metal-based spintronics is mainly applied for non-volatile memory devices or magnetic field sensors. A nonvolatile magnetic-random-access-memory (MRAM) using the GMR or TMR effect has been studied from 1990s, and MRAM indicates faster data processing speed and lower power consumption than a flash memory or dynamic-RAM (DRAM) [14]. However, 'high memory density' is an important key for a progress of the memory device, but this requirement is difficult due to high coercivity and crosstalk in the MRAM. Current-induced magnetization switching (CIMS) via spin-transfer torque (STT)

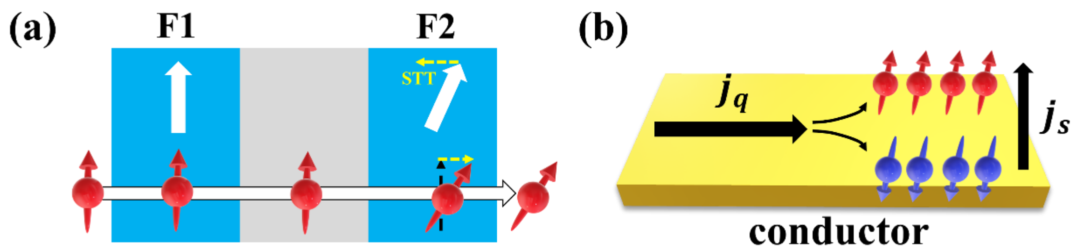

Figure 1-3 Schematic drawings for principles of (a) spin transfer torque (STT) and (b) spin hall effect (SHE).

discovered in 1996 has been researched to supplement those problems of MRAM, called STT-MRAM [15, 16, 17]. Figure 1-3 (a) shows schematic plots of the STT. The F2 ferromagnetic layer has a magnetization with an orientation tilted against that of F1. When a spin-polarized current is injected from the F1 into the F2, this electron-spin orientation becomes parallel to the magnetization of the F2. Continuously, a torque of this spin angular momentum is transferred to the magnetization by reaction, and it occurs a magnetization switching following the momentum conservation law. At this moment, the strength and the orientation of spin torque is determined by the spin-polarized current.

On the other hand, a two current model accounting for spin-dependent electron transport was proposed by Neville Mott in 1936 [18], and theoretical concept of spin current was defined. This model is that the density of current flowing in conductor consists of two current densities $\mathbf{j}_{\uparrow}$ and $\mathbf{j}_{\downarrow}$ induced by up- and down spins, respectively. The total current density is described by the sum of those two current densities $\mathbf{j_c} = \mathbf{j}_{\uparrow} + \mathbf{j}_{\downarrow}$. Their difference is defined as the spin current $\mathbf{j_s} = \mathbf{j}_{\uparrow} - \mathbf{j}_{\downarrow}$. The spin polarization of the spin-polarized current can be written as follows:

$$\mathrm{P} = \frac{|\mathbf{j}_{\uparrow} - \mathbf{j}_{\downarrow}|}{|\mathbf{j}_{\uparrow} + \mathbf{j}_{\downarrow}|} = \frac{\mathbf{j_s}}{\mathbf{j_c}}. \quad (1\text{-}3)$$

It was proposed by D’yakonov and Perel’ in 1971 that the spin current can be changed by the electrical current in a non-magnetic material via spin-orbit coupling, called an extrinsic spin-hall effect (SHE) [19, 20]. It is originated from the accumulation of spin-polarized electrons at two edges of the non-magnetic conductor when the electrical current $\mathbf{j_q}$ flows through a conductor. The spin current $\mathbf{j_s}$ flows perpendicular to $\mathbf{j_q}$ and is divided into up- and down-spin currents because of spin-orbit

interaction (SOI), as shown in Figure 1-3 (b). The strength of effective magnetic field in the SOI has different values depending on the spin direction, and this makes difference in probability of the scattering direction for the electron spin. It is well observed in heavy metals like Pb and Au with the strong spin-orbital interactions. The SHE has greatly contributed to the development of spintronics without a magnetic field. Meanwhile, direct electron-spin injection from the ferromagnet to semiconductor is difficult due to the conductivity mismatch or spin scattering at a junction or interface between them. To solve this problem, insulator tunnel barriers like ultrathin oxide films were introduced between the metal and semiconductor layers, or magnetic semiconductor layers were used instead of the ferromagnetic metal.

Magnetic semiconductors have been studied from 1960s because of no conductivity mismatch between a semiconductor and a magnet. Injection efficiency of 90 % from the magnetic semiconductor to non-magnetic one was obtained in BeMnZnSe of a II-VI compound diluted magnetic semiconductor (DMS), where magnetic elements of Mn replace a part of the non-magnetic ones in BeZnSe [21]. However, strong magnetic fields above several tesla and ultra-low temperatures are required to obtain the high injection efficiency. On the other hand, III-V compound magnetic semiconductors like GaMnAs and InMnAs have been proposed from 1990s, but there were some problems such as short spin lifetimes by hole doping and lower Curie temperature (T_c~110°C) than RT. To supplement these weaknesses of magnetic semiconductors, heterostructures with a ferromagnetic metal and non-magnetic semiconductor were introduced, e.g., ferromagnetic thin films such as Fe, Co deposited on semiconductor substrates or layers with sufficient high T_c and small coercivity.

Since the introduction of molecular beam epitaxy (MBE) in 1970s, semiconductor spintronics has made remarkable development leading to

new hetero- and nanostructures with atom-scale structural control. Finally, using semiconductor materials, several spin-based devices have been proposed as follows:

1) Spin field-effect-transistor (spin FET) is a device that can control electron-spin orientation using effective magnetic field induced by spin-orbit interaction in a semiconductor. Compared to conventional FET based on an electron charge, the energy for switching from 'OFF' to 'ON' state is only ~30 meV for spin FET [22]. Datta and Das first suggested a prototypical spin FET structure with a 2D electron gas channel and ferromagnetic source and drain contacts in 1990 [23]. The semiconductor channel needs a material with strong spin orbital interaction to control the direction of electron spin. Figure 1-4(a) and (b) show schematic structures of the spin FET when transistor is 'ON' and 'OFF', respectively. When an electrical current flows into the source contact, spin-polarized electron moves to the semiconductor channel. The orientation of electron spin is changed by the gate bias voltage, which can change the precession of spins by spin-orbit interaction in the

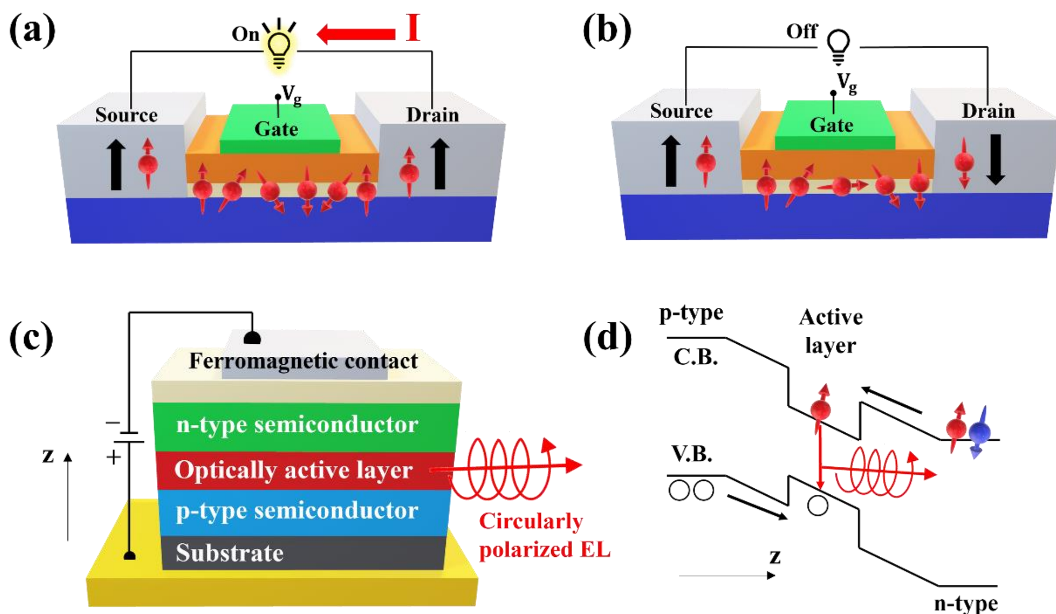

Figure 1-4 Schematic structures of spin FET when transistor is (a) 'ON' and (b) 'OFF'. A simple spin LED structure (c) and process of recombination (d).

semiconductor. If the electron-spin orientation in the channel is parallel to the magnetization direction of the drain contact, the drain current can flow (ON) and be detected. On contrary, there is no drain current (OFF) when the orientation of electron spin becomes anti-parallel to that of the drain. Therefore, the drain of spin FET can act as a spin-filter system.

2) Spin light-emitting-diode (spin LED) using p-type GaMnAs magnetic semiconductor was demonstrated by Y. Ohno et. al., based on spin injection and transport [24]. They achieved electron-spin injection into a semiconductor material with zero magnetic field and the hole spin transport over 200 nm. Recently, a non-magnetic semiconductor with a ferromagnetic thin film could be a key in the study of spin LED due to its long coherence time of electron spin. Figure 1-4 (c) and (d) indicate a simple schematic structure of the spin LED and a process of recombination between a spin-polarized electron and unpolarized hole. The spin-polarized electron via a ferromagnetic contact is injected into an optically active layer like quantum well (QW) or quantum dots (QDs) after transport through n-type semiconductor. After the recombination with a hole from p-type semiconductor, circularly polarized electro-luminescence (EL) was emitted from the optically active layer, as shown in Fig.1-4(d). Circularly polarized EL emitted from the device directly reflects the polarization of electron spin via a spin-conserved optical selection rule in the photoelectric conversion.

Spintronics is an ongoing technology, therefore it remains many assignments to realize practical spintronic devices. It is mainly considered with following three points to realize the spintronic devices [6]: (1) what is an efficient method for electron spin generation, (2) How long can the spin polarization be conserved during spin transport, (3) How to detect efficiently the spin-polarized electron without significant loss of spin information. In addition, it further needs new technology that

the orientation of electron spin, i.e., spin polarization, can be intentionally manipulated with an enough low power consumption before the spin detection.

1.3 Electron spin

After discovery of an electron using a cathode ray tube by J.J. Thomson in 1897, a concept of electron spin as an angular momentum, which is a fourth quantum number of the electron, was theoretically proposed by Wolfgang Pauli in 1925. At the same year, Uhlenbeck and Goudsmit who had studied the anomalous Zeeman effect discovered experimentally the electron spin [25]. In the Stern-Gerlach experiment, a silver-atom beam was split into two lines separated from each other when heterogenous magnetic field was applied, although the orbital magnetic moment of the silver atom is zero. They supposed that this was caused by the rotation of electron about its own axis, called as the spin magnetic moment. However, the electron spin is defined to the rotation of electron, but it differs from a classical concept of rotation. The electron spin has only a spin quantum number $s = 1/2$. The intrinsic spin angular momentum of electron and its z-component along the quantum axis are given by

$$S = \sqrt{s(s+1)}\hbar = \frac{\sqrt{3}\hbar}{2} \text{ and} \tag{1-4}$$

$$S_z = m_s\hbar = \pm\frac{\hbar}{2}, \tag{1-5}$$

as shown in Figure 1-5(a). Depending on the angular momentum, the electron spin has two directions with up- and down-spin, which has the z-projected spin quantum number m_s of $1/2$ and $-1/2$, respectively. By analogy with the depiction of the rotation of electron, an intrinsic magnetic dipole with a spin magnetic moment μ_s can be induced, as

follows:

$$\mu_s = -\frac{e}{2m_e} g_s S = \gamma S. \quad (1\text{-}6)$$

Here, m_e is an effective mass of electron. g_s indicates the spin g-factor and is approximately 2 for an electron [26]. The spin magnetic moment is proportional to the angular momentum with gyromagnetic ratio γ. It is important to understand an intrinsic spin-orbit interaction (in section 1.3.4) and an additional interaction with an external magnetic field (Zeeman splitting). Figure 1-5(b) indicates a schematic illustration of a rotational orbital movement of an electron associated with the spin. The rotation of the electron around a nucleus of atom can induce an orbital angular momentum $\boldsymbol{\ell}$. Therefore, a total angular momentum of rotating electron is defined by the sum of orbital and spin angular momenta, written as follows: $\mathbf{j} = \boldsymbol{\ell} + \mathbf{s}$. This should meet the conservation law of angular momentum. When applying an external magnetic field along the z-axis, the spin magnetic moment of electron is changed by generating a rotational force, called as a torque. This torque can be written with a magnitude of magnetic field $\mathbf{B}$, as follows:

$$\boldsymbol{\tau} = \frac{d\mathbf{j}}{dt} = \frac{1}{\gamma}\frac{d\boldsymbol{\mu}}{dt} = \boldsymbol{\mu} \times \mathbf{B}. \quad (1\text{-}7)$$

This motion of magnetic moment under a magnetic field is called as spin precession or Larmor precession, and it rotates with Larmor frequency $\omega = -\gamma B$ around the z-axis. In this process, the angular momentum is conserved therefore there is no change on spin states. On the other hand, the strength of the spin procession can be decayed as time goes on. This is originated from a loss of energy caused by lattice vibrations or some scattering processes, which results in electron spin orientation becomes parallel to the direction of applied magnetic field. This process is called

as spin damping, which is not a spin-conserving process. Therefore, the total torque during precession can be written from Landau-Lifshitz-Gilbert (LLG) equation as follows:

$$\frac{d\boldsymbol{\mu}}{dt} = \gamma\boldsymbol{\mu} \times \mathbf{B} - \frac{\alpha}{\mu}\left(\boldsymbol{\mu} \times \frac{d\boldsymbol{\mu}}{dt}\right), \tag{1-8}$$

where α is the Gilbert parameter associated with the precession rate of electron spin [27].

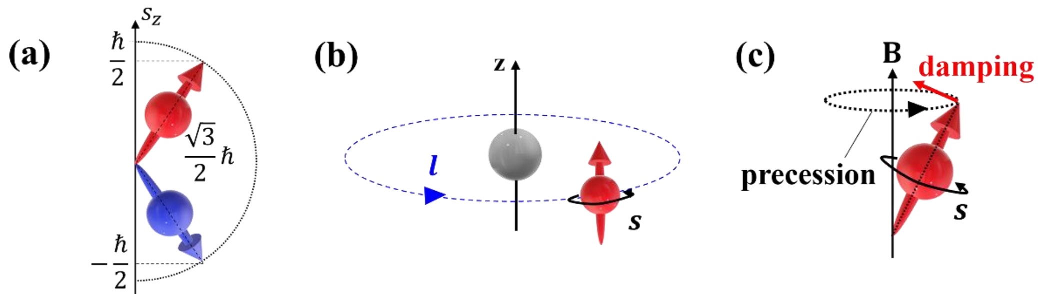

Figure 1-5 Schematic plots of (a) the angular momentum for electron spin, (b) some rotation movements associated with electron spin and (c) spin precession.

1.4 Generation of spin-polarized electron

Since an individual electron has essentially its spin direction with no external magnetic field, the generation of spin-polarized electrons indicates exactly that an imbalanced population between up- and down electron spins, which can be emerged by some methods. If the total number of up- and down spin is the same, there is no spin polarity because they cancel each other out. With the number of up- and down electron spin $N_{\uparrow,\downarrow}$, a nonequilibrium condition can be expressed in $N_{\uparrow} \neq N_{\downarrow}$, as shown in Figure 1-6 (a). In the case with $N_{\uparrow} > N_{\downarrow}$, the up spin is called “majority spin” while the other one is “minority spin”.

A spin-polarized electron is commonly generated by electrical or optical ways: 1) An electric current is a flow of spin-unpolarized electrons, which means that an electron spin density is under the

equilibrium state ($N_\uparrow = N_\downarrow$). When this current flows into ferromagnetic materials, the number of up- and down spin is unbalanced. In other words, electrons passed through ferromagnetic materials can be polarized, originating from the unbalanced state density of electron spin at near the fermi energy E_F in ferromagnetic metals, as shown in Figure 1-6 (b). The difference ($N_\uparrow - N_\downarrow$) between the densities of state for up- and down spin in ferromagnets can contribute to the saturation magnetization of conduction electrons and the spin polarization $P = (N_\uparrow - N_\downarrow)/(N_\uparrow + N_\downarrow)$ [28, 29]. In a ferromagnet/semiconductor coupled structure, spin-polarized electrons generated by the ferromagnet spreads into the semiconductor region, and it can induce spin diffusion within the spin-diffusion length limited by spin scattering.

2) Photoexcitation of spin-polarized electron was first experienced on silicon with optical pumping in 1968 [30]. Circularly polarized light makes an unbalanced number of spin-polarized electrons via the optical selection rule [31], as shown in Figure 1-6(c). The total angular momentum j has values as $|\ell - s| \leq j \leq \ell + s$, using the orbital angular momentum ℓ and spin angular momentum 's', as shown in Fig. 1-5(b). Furthermore, the optical selection rule is also represented by the magnetic quantum number m_j $(-j, -j+1, \cdots, j-1, +j)$, which is the total angular momentum projected on the z-axis as the quantum axis. In this model ($\ell = 0, 1$ for s, p-orbital and $s = 1/2$), the electron and hole states have the angular momentum with $j = 1/2$ and $j = 3/2$ at the conduction (C.B.) and valence bands (V.B.), respectively. The m_j values of electron are $+1/2$ and $-1/2$ for the up- and down spin, on

the other hand, the hole states are defined with $m_j = \pm 3/2$ for a heavy hole (HH) and $m_j = \pm 1/2$ for a light hole (LH) due to energy splitting of the valence band induced by their different effective masses [32]. Photons of circularly (left or right) polarized lights have momenta of $+1$ and -1. During absorption and emission of the circularly polarized lights, the total spin angular momentum of an electron-hole pair should be satisfied with $\Delta m_j = \pm 1$ according to the conservation law of angular momentum. The spin polarization is defined with a following equation:

$$P = \frac{N_P - N_{AP}}{N_P + N_{AP}} = \frac{I_P - I_{AP}}{I_P + I_{AP}}. \qquad (1\text{-}9)$$

Here, I_P and I_{AP} are PL intensities of circularly polarized lights, reflecting electrons with the spin parallel (P) and anti-parallel (AP) to the majority and minority spin generated after photoexcitation, respectively. The initial electron spin polarization was reported to be about 50 %

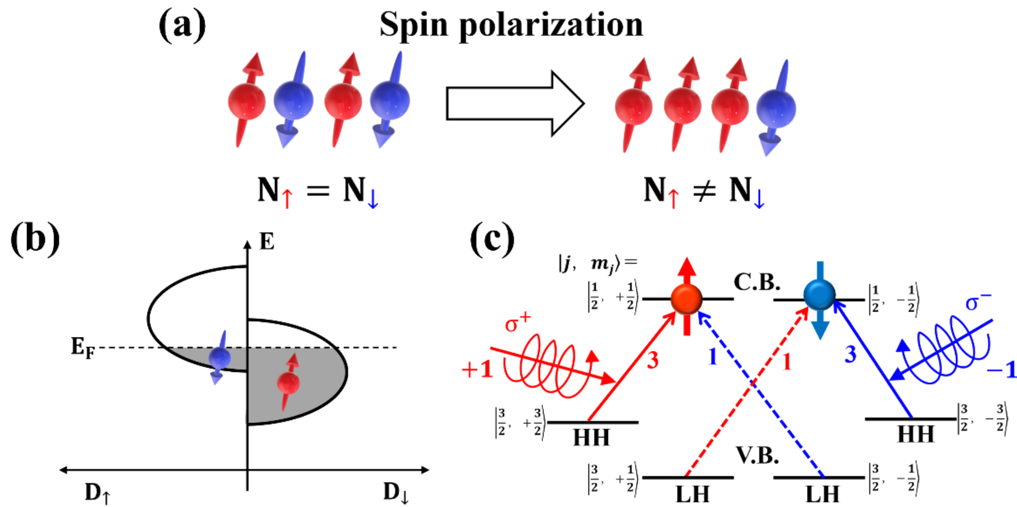

Fig.1-6 (a) Principle of spin polarization. The $N_\uparrow, N_\downarrow$ is the number of up- and down electron spin, respectively. (b) Band energy diagram of ferromagnetic metal. E_F is Fermi energy and $D_{\uparrow,\downarrow}$ indicates a density of state for up- and down electron spin (c) Schematic plot of optical selection rules during the absorption of circularly polarized light. The total angular momentum j and its projection on the z-axis m_j.

because the transition probability of the electron-HH pair is 3 times larger than that of electron-LH pair in a GaAs bulk [33].

1.5 Relaxation of electron spin

A nonequilibrium spin state returns to an equilibrium condition through some interaction and scattering mechanisms in conventional, i.e., non-magnetic semiconductors, and it is called as spin relaxation. There are three principal spin relaxation mechanisms in the semiconductor [6]: D'yakonov-Perel' (DP) [34, 35, 36], Elliott-Yafet (EY) [37, 38, 39] and Bir-Aronov-Pikus (BAP) [40, 41]. It is well-known that the BAP and DP mechanism is dominate at low and high temperatures in the semiconductor, respectively. Furthermore, the electron spin relaxes by the spin-orbit interaction (SOI), magnetostatic interaction, and hyperfine interaction and so on. The electron-spin relaxation time in bulk GaAs was observed with about tens of picoseconds at or above RT [42]. On the other hand, the relaxation time of the heavy-hole spin was reported to be ~110 fs due to the coupling of orbital-momentum with the angular momentum, so the hole spins, i.e., the spin polarization of hole, can be generally negligible in a bulk semiconductor [43].

1.5.1 D'yakonov-Perel' mechanism

The D'yakonov-Perel' (DP) spin relaxation mechanism arises from the Rashba or Dresselhaus spin-orbit interaction (SOI) leading to inversion asymmetry and spin splitting of a conduction band with the spin precession of electron. For example, the Rashba SOI is given by

$$\mathrm{H}_{\mathrm{RSO}} \sim \boldsymbol{\sigma} \cdot \boldsymbol{\Omega}(\mathbf{k}), \tag{1-10}$$

where $\boldsymbol{\sigma}$ is Pauli matrix and $\boldsymbol{\Omega}(\mathbf{k})$ is a vector of precession frequency. Due to the effective magnetic field, the spin-polarized electron undergoes

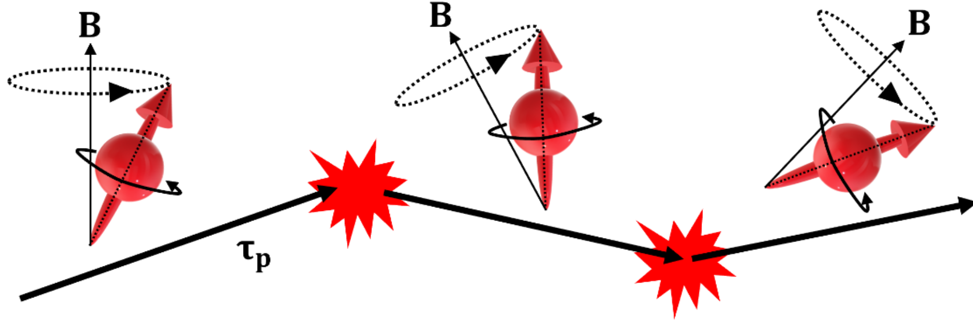

Figure 1-7 Schematic illustration of the DP spin relaxation. The direction of effective magnetic field **B** is changed by impurity or phonon scattering after a momentum scattering time $\boldsymbol{\tau_p}$.

precession with a frequency $\Omega(\mathbf{k})$ for a given momentum operator $\mathbf{k}$. However, the direction of effective magnetic field is changed during electron diffusion by impurity or phonon scattering in a semiconductor, as shown in Figure 1-7. Therefore, the phase of spin precession is randomized after collisions with the momentum scattering time τ_p. This phase transition of spin precession as a function of time can be expressed

$$\phi^2(t) = (\Omega_{av}\tau_p)^2 \frac{1}{\tau_p} t\,,$$

$$\phi^2(t) = {\Omega_{av}}^2 \tau_p t\,. \tag{1-11}$$

Here, Ω_{av} is an average of the precession frequencies. Since a time satisfying $\phi(t) \sim 1$ corresponds to a spin-relaxation time τ_s, the equation (11) can be written as follows:

$$1 \sim {\Omega_{av}}^2 \tau_p \tau_s\,,$$

$$\frac{1}{\tau_s} \sim {\Omega_{av}}^2 \tau_p\,. \tag{1-12}$$

In short, the spin-relaxation time τ_s is proportional to the inverse scattering time τ_p for this DP mechanism, as a following equation.

$$\tau_s \propto \frac{1}{\tau_p} \tag{1-13}$$

If the electron mobility decreases, the spin relaxation time τ_s will increases.

1.5.2 Elliott-Yafet mechanism

In small band-gap semiconductors, spin up and down states in a conduction band can be mixed, originating from their large spin orbit coupling. Thus, the Bloch function of mixed states using $\mathbf{k}\cdot\mathbf{p}$ perturbation theory can be written as follows:

$$\Psi_{\mathbf{k}n\uparrow}(\mathbf{r}) = [a_{\mathbf{k}n}(\mathbf{r})|\uparrow\rangle + b_{\mathbf{k}n}(\mathbf{r})|\downarrow\rangle]e^{i\mathbf{k}\cdot\mathbf{r}}$$
$$\Psi_{\mathbf{k}n\downarrow}(\mathbf{r}) = [a^*_{-\mathbf{k}n}(\mathbf{r})|\downarrow\rangle - b^*_{-\mathbf{k}n}(\mathbf{r})|\uparrow\rangle]e^{i\mathbf{k}\cdot\mathbf{r}}, \qquad (1\text{-}14)$$

where $|\uparrow\rangle$, $|\downarrow\rangle$ are two spin states with angular momenta of $\pm\frac{1}{2}$, and $a_{\mathbf{k}}$, $b_{\mathbf{k}}$ indicate components of the lattice symmetry matrix. Note, $\mathbf{k}$ is a vector of the lattice momentum and 'n' means band index. If there is momentum scattering with impurity or phonon, spin flip transition $\mathbf{k} \rightarrow \mathbf{k}'$ occurs probabilistically, as shown in Figure 1-8. The spin relaxation rate of this EY mechanism can be calculated from the probability of spin-flip transition. In III-V semiconductors, spin relaxation rate at energy $E_{\mathbf{k}}$ is given by [6, 39]

$$\frac{1}{\tau_s(E_{\mathbf{k}})} \sim A\Upsilon^2\left(\frac{E_{\mathbf{k}}}{E_g}\right)^2\frac{1}{\tau_p(E_{\mathbf{k}})}. \qquad (1\text{-}15)$$

Here, the numerical factor A is approximately 1. E_g, Δ_{SO} indicate the energy bandgap and spin-orbit splitting in a valance band, respectively. The Υ involves the Lande g-factor with a function of Δ/E_g. The EY spin relaxation mechanism strongly depends on temperature through $E_{\mathbf{k}}$, which is an energy considering momentum scattering in Eq. (1-15). The

main difference with the above DP mechanism is that a spin-relaxation time τ_s is proportional to scattering time τ_p for this EY effect.

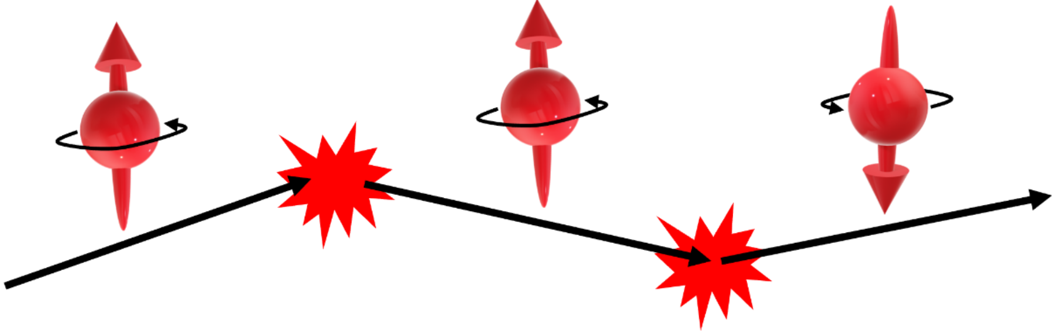

Figure 1-8. A schematic plot of EY spin relaxation mechanism. The spin flip occurs probabilistically by momentum scattering.

1.5.3 Bir-Aronov-Pikus mechanism

The Bir-Aronov-Pikus (BAP) mechanism is originated by the exchange interaction between an electron and hole. Therefore, it occurs strongly in heavily doped, especially p-doped semiconductors. The Hamiltonian of exchange interaction can be written as follows:

$$\mathrm{H} = \mathrm{D}\mathbf{J}\boldsymbol{\sigma}\delta(\mathbf{r})\delta(\mathbf{p},\mathbf{p}'). \qquad (1\text{-}16)$$

Note, 'D' is a constant of the exchange interaction, and $\mathbf{J}$ indicates the operator of angular momentum for a hole, and $\boldsymbol{\sigma}$ is the Pauli matrix for an electron. $\mathbf{r}$ is the difference of position between the electron and hole with $\mathbf{r} = \mathbf{r}_e - \mathbf{r}_h$, and $\mathbf{p}$ is their total angular momentum. The spin relaxation probability depends on the states of hole such as the presence of degeneracy. When there is the exchange interaction between an electron and nondegenerate holes, the spin relaxation rate is given by

$$\frac{1}{2\tau_s} = \frac{1}{\tau_0}\frac{v_e}{v_B}|\psi(0)|^4(Na_B{}^3), \qquad (1\text{-}17)$$

where τ_0 is an exchange splitting parameter, v_e and v_B is electron and

Bohr velocities with $v_B = \hbar/\varepsilon_e a_B$, where a_B is the exciton Bohr radius. 'N' indicates an acceptor density, and $|\psi(0)|^2$ is a Sommerfeld's factor. If hole state is degenerated and electron velocity is faster than the Fermi velocity of hole, the Eq. (1-17) changes as follows:

$$\frac{1}{2\tau_s} = \frac{3}{2}\frac{1}{\tau_0}\frac{v_e}{v_B}\frac{T}{\varepsilon_F}|\psi(0)|^4(Na_B{}^3). \qquad (1\text{-}18)$$

Here, ε_F is a hole energy at the Fermi level. In this BAP mechanism, a spin-relaxation time consequentially depends on the number of holes, carrier velocity and temperature.

1.5.4 Spin-orbit interaction

It is generally thought that the spin-polarized electron moves around the nucleus of an atom. However, from an electron's point of view, the atomic nucleus seems to be revolving around this spin-polarized electron. This orbital motion of nucleus with a positive electric charge makes virtually an orbital current (electric field) and then it generates an effective magnetic field H_{SO} at the location of the electron, resulting from the Biot-Sarvart law. Therefore, the spin magnetic moment of this electron interacts with this H_{SO}, and it is called as the spin-orbit interaction (SOI) [34]. That is, the SOI is a relativistic quantum mechanical effect. Figure 1-9(a) shows a schematic illustration of an orbital motion of a nucleus against for a spin-polarized electron with some vectors. The magnetic flux density $\vec{B}$ for the spin-polarized electron is depending on a velocity of the nucleus $\vec{\upsilon}$ and the induced electric field $\vec{E}$ [44], so it is given by

$$\vec{B} = -\frac{1}{c^2}\vec{\upsilon} \times \vec{E}. \qquad (1\text{-}19)$$

Note, c is a velocity of light. From the equation (1-19) with $\vec{E}$ which is

induced by the orbital motion of a nucleus,

$$\vec{E} = \frac{Ze}{4\pi\varepsilon_0}\frac{\vec{r}}{r^3} \tag{1-20}$$

The magnetic flux density $\vec{B}$ can be written by

$$\vec{B} = \frac{Ze}{4\pi\varepsilon_0}\frac{\vec{r}\times\vec{v}}{c^2r^3}. \qquad (\vec{\ell} = \vec{r}\times m\vec{v})$$

$$\vec{B} = \frac{1}{4\pi\varepsilon_0}\frac{Ze}{c^2mr^3}\vec{\ell}. \tag{1-21}$$

Here, ε_0 is vacuum permittivity and 'm' is a mass of an atom. 'r' is a radius when a nucleus does a circular movement around the electron. The $\vec{B}$ is perpendicular to $\vec{E}$ and parallel to the orbital angular momentum $\vec{\ell}$. The effective magnetic field H_{SO} applied to the spin-polarized electron by SOI is defined from eq. (1-6) and (1-21), and therefore,

$$H_{SO} = -\vec{\mu_s}\cdot\vec{B},$$

$$H_{SO} = \frac{1}{4\pi\varepsilon_0}\frac{Ze^2}{c^2m^2r^3}\vec{\ell}\cdot\vec{s}. \tag{1-22}$$

This is derived from the Dirac equation for relativistic case [45]. The strength of SOI is proportional to the atomic number.

In a system with time-reversal and inversion symmetries, each energy

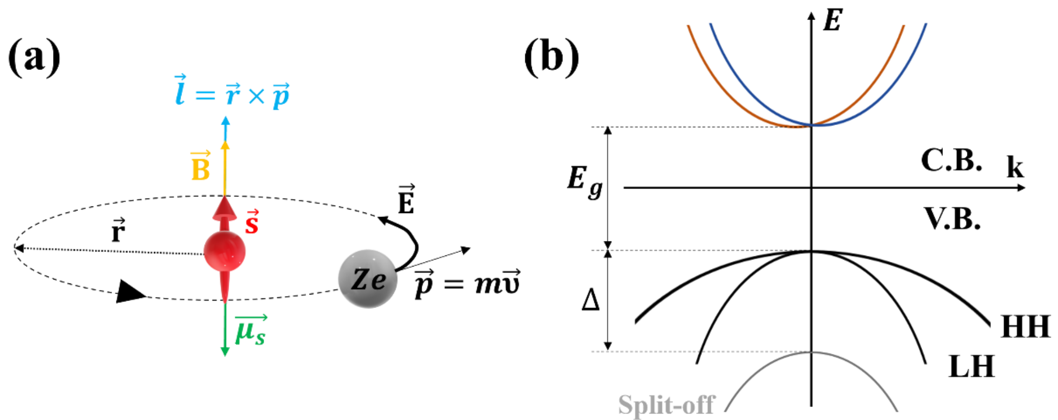

Figure 1-9 (a) A schematic illustration of the orbital motion of a nucleus. (b) Band splitting induced by SOI.

eigenstate is at least doubly degenerate for an odd number of spins. This is so-called Kramers degeneracy, and it can be written as follows: $E(\mathbf{k},\uparrow) = E(\mathbf{k},\downarrow)$, where $\mathbf{k}$ is a wavevector. However, if inversion symmetry in a system is broken with SOI, a conduction band splitting can be introduced for the p-orbital with the breaking of Kramers degeneracy, as shown in Figure 1-9(b). At this moment, the energy splitting is given by [35]

$$\hbar\Omega = 2\alpha\kappa(8m_c^3E_g)^{-1/2}, \tag{1-23}$$

where κ is the spin components along the direction of a vector $\boldsymbol{\kappa}$. Note, α is a certain coefficient indicating the strength of SOI, and m_c is a mass of electron in a conduction band, E_g is a band-gap energy, Ω is a precession frequency in a specific magnetic field along $\boldsymbol{\kappa}$. The SOI also results in spin-orbit splitting in a valence band with energy Δ, depending on the magnitude of SOI.

In III-V compound semiconductors, there are Dresselhaus and Rashba SOIs built by bulk inversion asymmetry (BIA) and surface inversion asymmetry (SIA), respectively [46-48]. The lack of the inversion symmetry creates an internal electric field perpendicular to the in-plane direction, leading to an effective magnetic field in Eq. (1-19). As a result, the spin degeneracy can be lifted. For reference with Eq. (1-23), different functions of κ are given for Dresselhaus (1-24a) and Rashba SOI (1-24b), as follows:

$$\kappa = \left\{k_x\left(k_y^2 - k_z^2\right), k_y(k_z^2 - k_x^2), k_z(k_x^2 - k_y^2)\right\} \tag{1-24a}$$

$$\kappa = (k_y, -k_x) \tag{1-24b}$$

Finally, electron-spin manipulations without external magnetic fields can be possible by controlling the strength of SOI, and it may lead to

realize a spin FET. The control of SOI strength using an electric field effect is achieved by Y. Kanai et al. in 2011 [49]. They reported that the energy of SOI with a wide range of 50~150 μeV can be controlled by a side-gate bias voltage in a single InAs self-assembled quantum dot. However, SOI also contributes to the spin relaxation with the enhanced DP mechanism, so the electrically precise tuning of SOI is requested for device applications.

1.6 Semiconductor quantum dot

A semiconductor quantum dot (QD) is a zero-dimensional nanostructure with several or tens of nm in diameter. Since a wave function of a microscopic particle is confined in this nano-space, the QD has a specific de Broglie wavelength and discrete energy level by its strong 3D quantum confinements. Figure 1-10 indicates schematic drawings of the density of the state (DOS) in (a) a bulk, (b) a quantum well (QW) and (c) a QD. An eigenvalue of an energy for electron in a bulk is given by

$$E_k = \frac{\hbar^2}{2m}\left(k_x{}^2 + k_y{}^2 + k_z{}^2\right),$$

and the DOS in a bulk $\rho(E)_{bulk}$ is written by

$$\rho(E)_{bulk} = \frac{1}{2\pi^2}\left(\frac{2m^*}{\hbar^2}\right)^{\frac{3}{2}}\sqrt{E}.$$

That is, the bulk DOS is proportional to $\sqrt{E}$. In the case of 2D-QW, the energy of an electron trapped in z-direction has discrete quantum levels $\varepsilon_{\mathbf{zn}}$ $(n = 1, 2, 3\ \cdots)$, as follows:

$$E_{\mathbf{zn}}\left(k_x, k_y\right) = \frac{\hbar^2}{2m^*}\left(\frac{2\pi}{L}\right)^2\left(n_x{}^2 + n_y{}^2\right) + \varepsilon_{\mathbf{zn}} \equiv E_{xy} + \varepsilon_{\mathbf{zn}}.$$

The DOS for a QW with surface area S (the square of the length L of one side in a QW) is written by

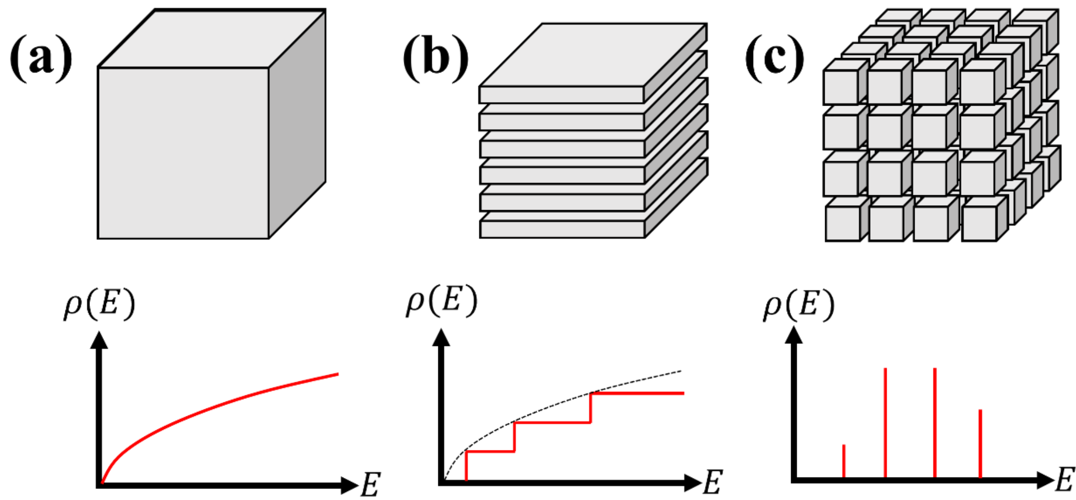

Figure 1-10 Schematic drawings of (a) a bulk, (b) QWs and (c) QDs indicating with each density of the states (DOS).

$$\rho(E)_{well} = \frac{m^*S}{\pi\hbar^2},$$

and this DOS has a constant value regardless of the energy within the same ε_{zn}. On the other hand, the DOS in a 0D-QD is written by a following equation:

$$\rho(E)_{dot} = 2\delta(E - \varepsilon_{xyzn}).$$

Therefore, this DOS has an infinite value against a quantum level ε_{xyzn},

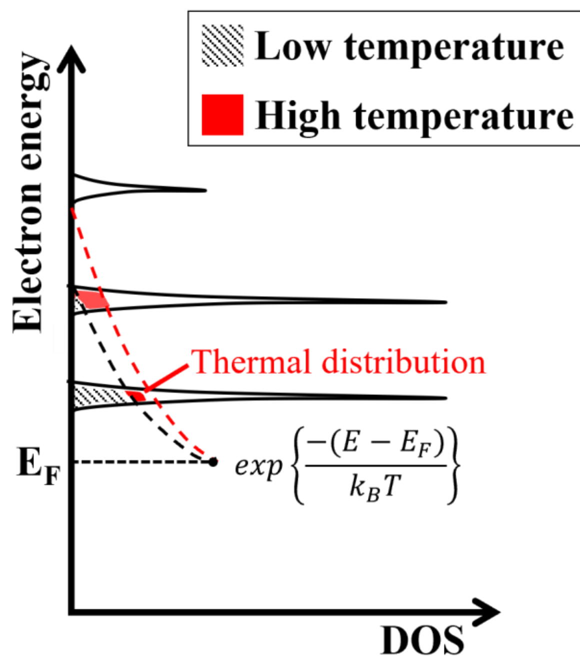

Figure 1-11 Thermal distribution of electrons in QDs with lower and higher temperatures.

which determines levels for each direction. That is, the DOS of the QD can be expressed by a delta function, as illustrated in Figure 1-11. This means that the thermal distribution of electrons is less sensitive to external environmental temperatures, so it is possible to develop a temperature insensitive QD laser with an ultralow-threshold current [50, 51]. Figure 1-12 shows (a) a schematic drawing of the quantum confinement in a QD, (b) a typical high-angle annular dark-field scanning transmission electron microscopy (HAADF-STEM) image of a cross-sectional InGaAs QD structure. This semiconductor QD is grown on a wetting layer (WL) with the Stranski-Krastanow (SK) growth mode by molecular beam epitaxy (MBE). Electronic and optical properties of the QD depend on its size and shape, which are controlled by growth conditions such as a growth temperature and As partial pressure [52, 53]. Figure 1-12(c) indicates a schematic band structure of the QD and the corresponding luminescent process. After spin-polarized electrons and holes are simultaneously injected from the excited state (ES) into the ground state (GS) by energy relaxation, circularly polarized photoluminescence (PL) can be emitted from the QD-GS via recombination between a pair of electrons and holes.

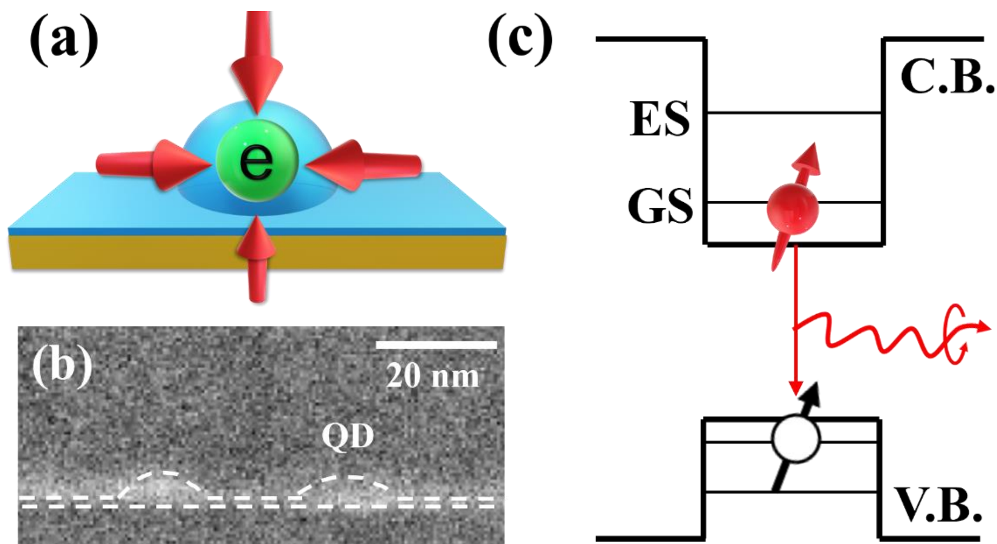

Figure 1-12. (a) A schematic drawing of the quantum confinement in QD. (b) A typical high-angle annular dark-field scanning transmission electron microscopy (HAADF-STEM) image of a cross-sectional QD structure. (c) Schematic band structure of QD and the corresponding luminescent process.

At this moment, spin polarization degree of electrons is reflected in circularly polarization degree of emitted PL according to the optical selection rules.

In conventional bulk semiconductors, spin-polarized electrons interact frequently with impurities or other carriers during their movements, easily leading to spin depolarization. On the contrary, electron-spin relaxation, especially DP spin relaxation mechanism, can be significantly suppressed in QDs because the movement of electrons is rather restricted by their strong quantum confinements. For example, a spin lifetime was reported to be up to 1 ms for a single electron in self-assembled Ga(In)As QDs [54]. Furthermore, in QDs, the spin orientation (polarity) of carriers is potentially able to be manipulated because of a small number of carriers in this QDs. Therefore, QDs are a one of the most promising materials to realize new opto-spintronic devices such as a spin LED or spin transistor.

Bibliography

[1] K. K. Young, IEEE Transactions on Electron Devices **36**, 99-109 (1989).

[2] A. Chaudhry and M. J. Kumar, IEEE Trans. Device Mater. Reliab. **4,** 569 (2004).

[3] R. D. Isaac, IBM J. Res. Dev. **44**, 369-378 (2000).

[4] C. A. Mack, IEEE Trans. Semicond. Manuf. **24**, 202-207 (2001).

[5] S. Xi, American Scientist **89**, 516-523 (2001).

[6] I. Zutic, J. Fabian, and S. D. Sarma, Rev. Mod. Phys. **76**, 323 (2004).

[7] M. Julliere, Phys. Lett. **54A**, 225-226 (1975).

[8] R. Meservey, P. M. Tedrow, and J. S. Moodera, J. Magn. Magn. Mater. **35**, 1-6 (1983).

[9] M. N. Baibich, J. M. Broto, A. Fert, F. N. V. Dau, F. Petroff, P. Etienne, G. Creuzet, A. Friederich, and J. Chazelas, Phys. Rev. Lett. **61**, 2472 (1988).

[10] J. S. Moodera, L. R. Kinder, T. M. Wong, and R. Meservey., Phys. Rev. Lett.

74, 3273 (1995).

[11] G. Li, S. Sun, R. J. Wilson, R. L. White, N. Pourmand, and S. X. Wang, Sens. Actuators A: Phys. **126**, 98-106 (2006).

[12] A. V. Silva, D. C. Leitao, J. Valadeiro, J. Amaral, P. P. Freitas, and S. Cardoso, Eur. Phys. J. Appl. Phys. **72**, 10601 (2015).

[13] S. Yuasa, T. Nagahama, A. Fukushima, Y. Suzuki, and K. Ando, Nature Materials **3**, 868-871 (2004).

[14] S. Tehrani, J. M. Slaughter, E. Chen, M. Durlam, J. Shi, and M. DeHerrera, IEEE Trans. Magn. 35, 2814-2819 (1999).

[15] J. C. Slonczewski, J. Magn. Magn. Mater. **159**, L1-L7 (1996).

[16] Y. Huai, AAPPS Bulletin **18**, 33 (2008).

[17] F. J. Albert, J. A. Katine, R. A. Buhrman, and D. C. Ralph, Appl. Phys. Lett. **77**, 3809 (2000).

[18] N. F. Mott, Proc. Roy. Soc. **A153**, 699 (1936).

[19] M. I. Dyakonov and V. I. Perel, Sov. Phys. JETP Lett. 13, 467 (1971).

[20] M. I. Dyakonov and V. I. Perel, Phys. Lett. A **35**, 459 (1971).

[21] R. Fiederling, M. Keim, G. Reuscher, W. Ossau, G. Schmidt, A. Waag, and L. W. Molenkamp, Nature **402**, 787-789 (1999).

[22] S. Luryi, J. Xu, and A. Zaslavsky, 'Future Trends in Microelectronics: Frontiers and Innovations', Technology & Engineering (2013).

[23] S. Datta and B. Das, Appl. Phys. Lett. **56**, 665 (1990).

[24] Y. Ohno, D. K. Young, B. Beschoten, F. Matsukura, H. Ohno, and D. D. Awschalom, Nature **402**, 790 (1999).

[25] G. E. Uhlenbeck and S. Goudsmit, Nature **117**, 264-265 (1926).

[26] B. Odom, D. Hanneke, B. D'Urso, and G. Gabrielse, Phys. Rev. Lett. **97**, 030801 (2006).

[27] T. L. Gilbert, IEEE Trans. Magn. **40**, 3443-3449 (2004).

[28] R. Meservey, D. Paraskevopoulos, and P, M. Tedrow, Phys. Rev. B **22**, 1331 (1980).

[29] M. B. Stearns, J. Magn. Magn. Mater. **5**, 167 (1977).

[30] G. Lampel, Phys. Rev. Lett. **20**, 491 (1968).

[31] R. C. Miller and D. A. Kleinman, J. Lumin. **30**, 520-540 (1985).

[32] A. L. Mears and R. A. Stradling, J. Phys. C **4**, L22 (1971).

[33] S. Pfalz, R. Winkler, T. Nowitzki, D. Reuter, A. D. Wieck, D. Hagele, and M. Oestreich, Phys. Rev. B **71**, 165305 (2005).

[34] M. I. Dyakonov, 'Spin Physics in Semiconductors', Springer (2008).

[35] M. I. Dyakonov, and V. I. Perel, Sov. Phys. JETP **33**, 1053 (1971).

[36] L. Szolnoki, A. Kiss, B. Dora, and F. Simon, Sci. Rep. **7**, 9949 (2017).

[37] R. J. Elliott, Phys. Rev. **96**, 266 (1954).

[38] A. Kiss, L. Szolnoki, and F. Simon, Sci. Rep. **6**, 22706 (2016).

[39] J. N. Chazalviel, Phys. Rev. B **11**, 1555 (1975).

[40] A. G. Aronov, G. E. Pikus, and A. N. Titkov, Sov. Phys. JETP **57**, 680 (1983).

[41] G. L. Bir, A. G. Aronov, and G. E. Pikus, Zh. Eksp. Teor. Fiz. **69**, 1382 (1975) [Sov. Phys. JETP **42**, 705 (1975)].

[42] S. Oertel, J. Hubner, and M. Oestreich, Appl. Phys. Lett. **93**, 132112 (2008).

[43] D. J. Hilton and C. L. Tang, Phys. Rev. Lett. **89**, 146601 (2002).

[44] L. H. Thomas, Nature **117**, 514 (1926).

[45] P. A. M. Dirac, "The Quantum Theory of the Electron", Royal Society **117**, 610 (1928).

[46] G. Dresselhaus, Phys. Rev. **100**, 580 (1995).

[47] M. Kohda, T. Bergsten, and J. Nitta, J. Phys. Soc. Jpn. **77**, 031008 (2008).

[48] J. P. Eisenstein, H. L. Stormer, V. Narayanamurti, A. C. Gossard, and W. Wiegmann, Phys. Rev. Lett. **53**, 2579 (1984).

[49] Y. Kanai, R. S. Deacon, S. Takahashi, A. Oiwa, K. Yoshida, K. Shibata, K. Hirakawa, Y. Tokura, and S. Tarucha, Nat. Nanotechnol. **6**, 511 (2011).

[50] Y. Arakawa and H. Sakaki, Appl. Phys. Lett. **40**, 939 (1982).

[51] P. G. Eliseev, H. Li, A. Stintz, G. T. Liu, T. C. Newell, K. J. Malloy, and L. F. Lester, Appl. Phys. Lett. **77**, 262 (2000).

[52] T. Yamamura, T. Kiba, X. Yang, J. Takayama, A. Subagyo, K. Sueoka, and A. Murayama, J. Appl. Phys. **116**, 094309 (2014).

[53] C. Y. Ngo, S. F. Yoon, C. Z. Tong, W. K. Loke, and S. J. Chua, Nanotechnology **18**, 365708 (2007).

[54] M. Kroutvar, Y. Ducommun, D. Heiss, M. Bichler, D. Schuh, G. Abstreiter, and J. J. Finley, Nature **432**, 81 (2004).

Chapter 2. Research purpose

2.1 Background

2.1.1 Spin injection in QW/QD tunnel-coupled nanostructures

Efficient spin injection into QDs is one of the most important subjects for optical spin devices. It is not suitable for generation of spin-polarized electrons directly in the QDs, leading to a spin-state filling effect that makes the electron-spin polarization significantly lower. In addition, electron-spin polarization can relax during transport particularly at RT before the injection into the QD. Therefore, one needs additional layers to suppress the spin relaxation of electrons and smoothly and effectively inject them into the QDs. QW/QD tunnel-coupled nanostructures were introduced to suppress the electron-spin relaxation during spin transport and injection processes. This QW/QD coupled nanostructures can be a source of ultrafast spin injection via quantum tunneling basically without spin relaxation originated from an overlap of electron wavefunctions between the QW and QD [1-3]. The efficiency of the electron-spin conservation during the injection from the QW into the QDs was higher than 90 %. In this structure, a self-assembled QD layer is coupled with a QW layer by ultrathin tunneling barrier, and the QW layer acts as a reservoir of spin-polarized electrons photoexcited. Since the energy state

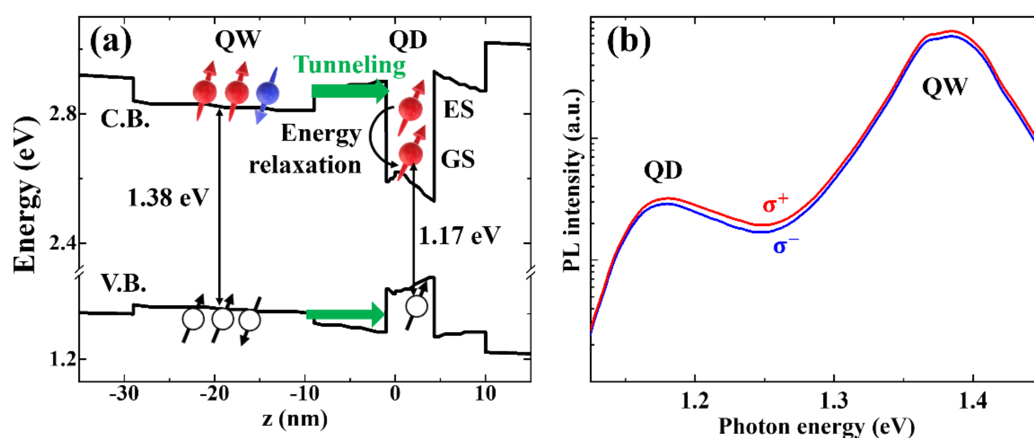

Figure 2-1 (a) A schematic plot of energy band and (b) the PL spectrum as a function of photon energy in QW-QD coupled structure.

of an electron initially excited at the QW is slightly higher than the energy of one of excited states (ESs) at the QD, spin-polarized electrons can be immediately injected into the QD via energy relaxation via the longitudinal optical (LO)-phonon scattering during tunneling, i.e., LO-assisted quasi-resonant tunneling [13]. This fast energy relaxation contributes to high spin polarizations due to the suppressed spin relaxation. Figure 2-1 (a) indicates a schematic plot of calculated energy band along the growth direction (QW→QD; z-direction) in the QW-QD coupled nanostructure. This potential diagram of the energy band was calculated using the Nextnano simulator [4]. Exited electron and hole spins are injected from the QW into the QD ES via spin conserved tunneling, and then they simultaneously relaxed to the ground state (GS) of the QD by emitting phonons. During this process, circularly polarized PL is observed at RT in this QW-QD nanostructure, as shown in Figure 2-1(b). Here, σ^+ and σ^- indicate co- and cross circularly polarized PL (luminescence with parallel and antiparallel spins to the initial spin generated just after photoexcitation) under σ^+-polarized excitation, respectively. Two PL peaks at 1.17 and 1.38 eV correspond to energy-band gaps between the electron and hole spins at the GS of the QD and the QW in Fig. 2-1(a). Due to the different density of the states between the QW and QD, the PL intensities of the energy region arise from the QW are higher than those of QD.

Spin injection efficiency between the QW and the QDs depends on the exciton energy [2], the thickness of tunneling barrier as well as the QW [5, 6]. This spin-injection efficiency determines the initial spin polarization at the QD when spin-polarized electrons are just injected into the QD-ES. It is reported that ultrafast (5-20 ps) spin injection with different barrier thicknesses (2-8 nm) is demonstrated in an InGaAs QW/QD coupled

nanostructures [5]. Furthermore, as a tunneling barrier thickness was thinner, spin injection time is faster leading to high spin polarizations induced by the suppressed spin relaxation during the injection.

2.1.2 Spin manipulation using electric field

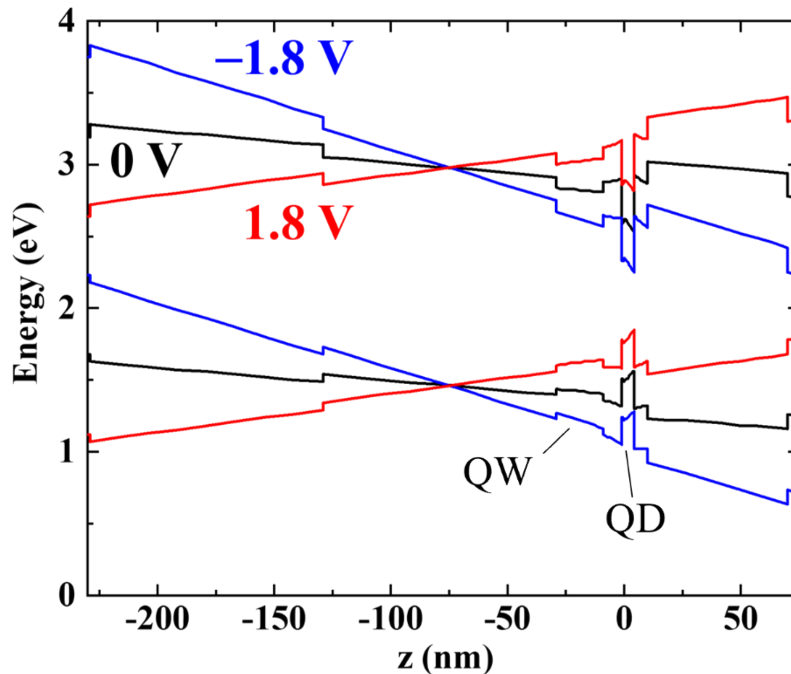

Figure 2-2 Calculated 1D potential of energy band in a QW/QD nanostructure at external biases of −1.8, 0 and 1.8 V.

An electric-field effect on an electron-spin polarization has been studied as a new attempt for the purpose of spin manipulation [9, 10, 12]. For QW/QD coupled nanostructures, applying an external electric field induce potential modifications. Optical spin devices using InGaAs QW/QD coupled nanostructures were fabricated, and the band energy with varied bias voltages was calculated, typically as shown in Figure 2-2. The external electric field is applied along the growth direction (QW→QD; z-direction). A band potential is close to flat at around 0 V, where both spin-polarized electrons and holes can be injected efficiently into the QDs. However, spin-polarized electrons start to localize in the QW due to the potential tilted towards the QW side when a positive voltage is applied like

+1.8 V, while the injection of the holes into the QD can be accelerated. At negative bias voltage of −1.8 V, the band energy of the QD decreases inducing the enhanced electron-spin injection toward the QD side. Figure 2-3 shows 3D calculated electron wavefunctions of the QW/QD coupled structures with bias voltages of (a) −1 and (b) 1 V. The blue and green areas in Fig. 2-3 indicate the existence probabilities of an electron. In the case of 0 V, the wavefunction at the first excited state (ES) of the QD is coupled with the GS of the QW. At a negative bias of −1 V, electrons are localized in the QD as stated above, therefore the existence probability of electron is very high at the QD-GS. However, the wavefunction of electron is observed faintly at the ES of QD with a bias voltage of +1 V. This is because the potential slightly tilts toward the QD side in this sample.

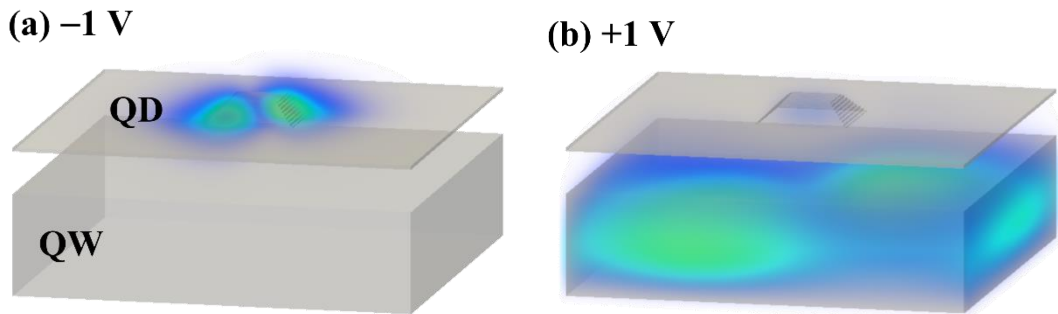

Figure 2-3 3D calculated electron wavefunctions in the QW/QD coupled nanostructure with (a) −1 and (b) 1 V. The blue and green areas indicate the existence probability of an electron.

Figure 2-4 indicates the bias dependence of the PL intensity obtained from the QD-GS at 4 K in InGaAs QW/QD coupled nanostructures. The PL intensity peak is observed in the range of 0 ~ 1 V, where both electrons and holes are efficiently injected into the QDs with their number ratio of 1:1, approximately. Below 0 V, the PL intensity decreases due to the lack of holes in the QDs whereas the injection of electrons can be enhanced, where the conduction-band potential tilts toward the QD side. On the other hand, the number of electrons in the QDs becomes insufficient above 1 V, resulting in the decreased PL intensity. These results show that electric

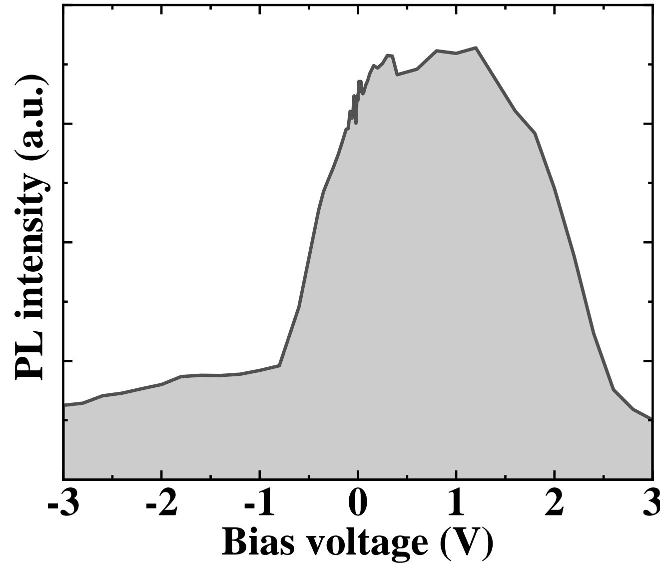

Figure 2-4 Bias dependence of the PL intensity at the QD-GS in InGaAs QW/QD coupled nanostructures at 4 K.

field can control the injection dynamics of carriers from the QW into the QDs.

2.1.3 Spin flip scattering

One can assume that there is one electron with the majority (up state) spin at the GS of the QD when a hole is absent in a valence band, as shown in Figure 2-5(1). This spin-polarized electron remained at the QD-GS is called a residual electron, and one assumes that its spin is parallel to the majority spin initially excited at the QW. A spin-polarized electron with parallel to that of the initial majority spin is continuously injected into the QD [Fig. 2-5(2)], however the injected electron cannot relax to the QD-GS via the Pauli's exclusion principle as far as the residual electron exists, as shown in Fig. 2-5(3). Continually, hole with slow injection time compared to that of electron is injected into the QD-ES. At this time, if spin-polarized hole exists at the same excited state with the same spin orientation of the injected electron, spin states of an electron-hole pair can simultaneously be reversed, i.e., flipped, originating from the enhanced electron-hole exchange interaction confined in the QD space [Fig.2-5(4)],

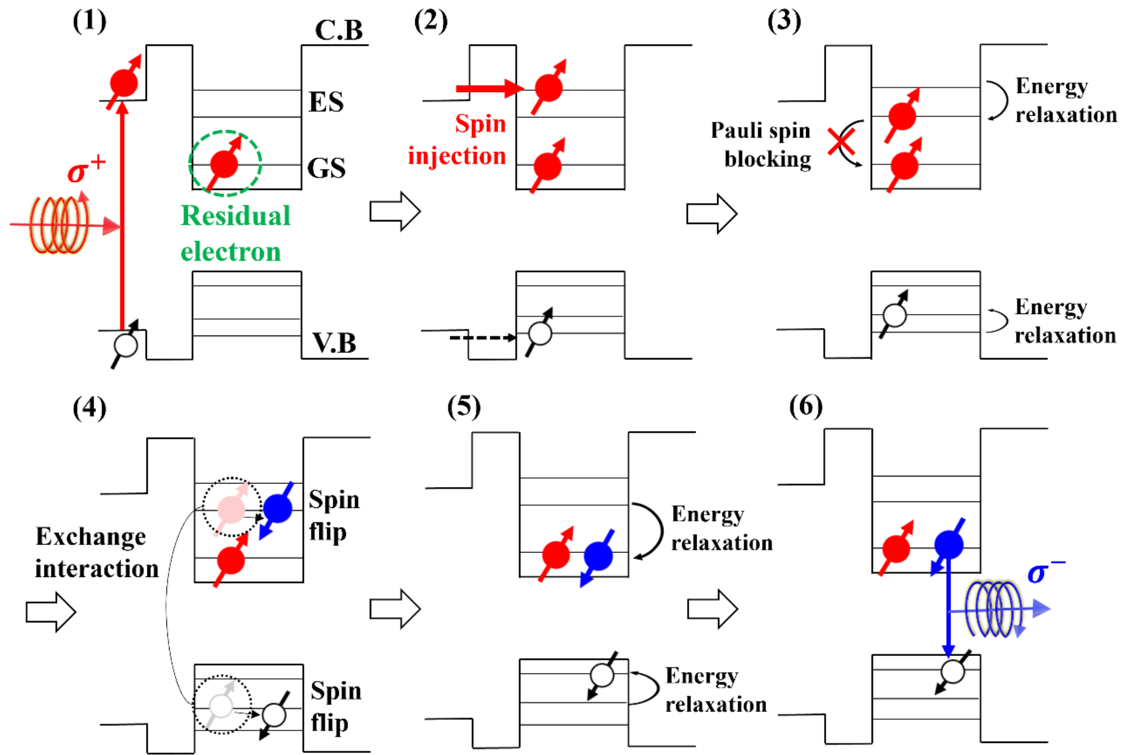

Figure 2-5 Schematic illustrations for the mechanism of the spin-flip scattering in the QD.

and then they can relax into the GS with anti-parallel spin direction against the spin state of the residual electron as well as the initial spins [Fig.2-5(5)]. This series of process is named spin flip scattering [7, 8] The number ratio of the electron to hole is 2:1 at the QD-GS in this model illustrated in Fig. 2-5(6). For this process to occur, electron-hole exchange scattering must occur at the instant before the spin-polarized hole relaxes its energy to the QD-GS. If such spin-flip scattering is dominant, the PL polarization observed in the QD will be negative as in equation (1-9).

According to the previous studies [9, 10, 12], this spin-flip scattering was observed at specific bias conditions, where the electron-spin injection into the QDs was enhanced. Figure 2-6 (a) and (b) show circularly polarized QD-PL spectra and the corresponding the spin polarization degree with a bias voltage of 0.2 V and the bias dependence of the spin polarization degree at the QD-GS at 4 K in a QW/QD coupled nanostructure, respectively. Here, $\sigma^{\pm}$ indicates $\sigma^{\pm}$-circularly polarized

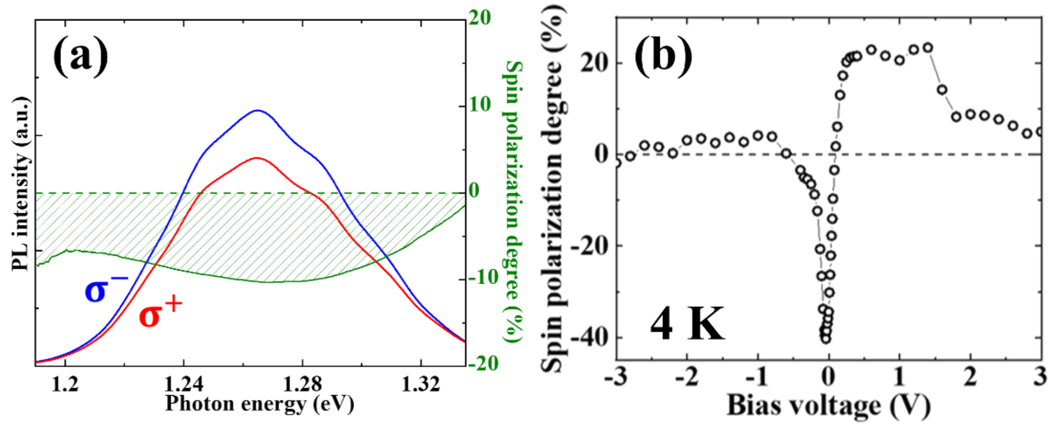

Figure 2-6 (a) Circularly polarized QD-PL spectra and the corresponding spin polarization degree with a bias voltage of 0.2 V and (b) bias dependence of spin polarization at low temperature in the QW/QD coupled nanostructure.

PL under σ^+-polarized excitation. The PL intensity peak in Fig. 2-6(a) appears at 1.26 eV, mainly originated from the QD-GS emission. The PL intensity of σ^- is higher than that of σ^+ in this plotted range of photon energy. The spin polarization degree indicates the maximum negative value of −10 % calculated with the equation (1-9). This result is originated from the abovementioned spin-flip scattering at the QD-ES1. The spin polarization degree also largely depends on applied bias voltage, as shown in Fig. 2-6(b). The spin-flip scattering is dominant at around 0 V, where the residual electron remains at the QD-GS. Below –0.5 V, the spin polarization degree becomes almost zero owing to the suppressed hole-spin injection into the QDs, whereas spin-polarized electrons start to escape from the QD to the QW. The bias-voltage condition, where the spin-flip scattering occurs, varies significantly with hole concentration [10], supporting this spin-flip mechanism depending on the existence of the residual electron in the QD-GS, the device structure, and others.

2.2 Research purpose

Electron-spin manipulation using an external electric field in conventional non-magnetic semiconductor materials has been studied so

far only at low temperatures, for instance, in the above electric-field-effect optical spin devices using QW/QD coupled nanostructures [9, 10]. It was reported that the electron spin polarization and polarity can be controlled by bias voltages, which change the relative number of injected spin-polarized electron and hole depending on the strength and direction of the applied electric field. However, it is necessary to understand electron-spin dynamics at high temperatures for the purpose of practical RT operation of this kind of opto-spintronic device. Figure 2-7 shows a schematic mechanism for thermal escape of a spin-polarized electron from a QD. As temperature increases, the spin-polarized electron at the QD-GS can be excited to the higher ESs or escape thermally from the QD. As a result, PL intensity emitted from the QD decreases and the value of the spin polarization degree also drops owing to the re-injection of a spin-depolarized electron after thermal escape and subsequent migration in barriers [11]. Therefore, new attempts are strongly demanded for maintaining high spin polarization and controlling spin polarity by means of an external electric field at high temperatures including RT.

In this study, I have investigated temperature dependences of the spin polarization and electric-field effect on the electron spin dynamics at RT in InGaAs QW/QD coupled nanostructures [12]. Furthermore, I have also focused on the bias dependences of the electron-spin polarization and resulting circularly polarized PL emissions in newly developed InAs

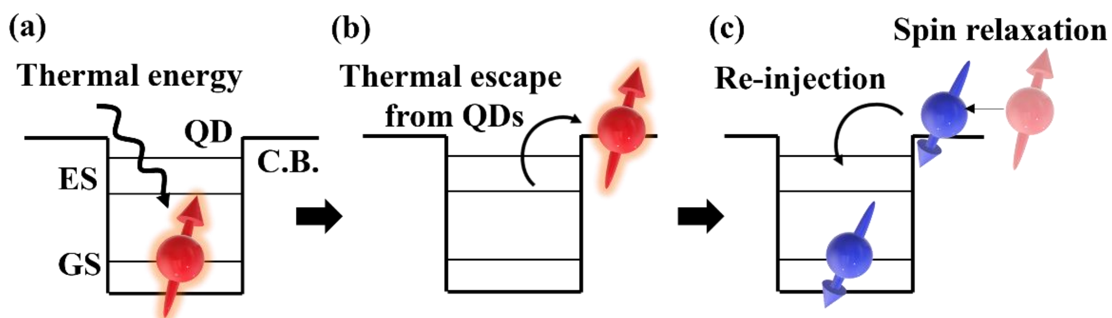

Figure 2-7 A schematic mechanism for thermal escape of electron spin from a QD.

QD tunnel-coupled nanostructures with employing a GaNAs QW as well as an InGaAs QW at different temperatures up to RT, respectively.

Bibliography

[1] A. Murayama, T. Asahina, K. Nishibayashi, I. Souma, and Y. Oka, Appl. Phys. Lett. **88**, 023114 (2006).

[2] A. Murayama, T. Furuta, K. Hyomi, I. Souma, Y. Oka, D. Dagnelund, I. A. Buyanova, and W. M. Chen, Phys. Rev. B **75**, 195308 (2007).

[3] D. Dagnelund, I. A. Buyanova, W. M. Chen, A. Murayama, T. Furuta, K. Hyomi, I. Souma, and Y. Oka, Phys. Rev. B 77, 035437 (2008).

[4] S. Birner, T. Zibold, T. Andlauer, T. Kubis, M. Sabathil, A. Trellakis, and P. Vogl, IEEE Trans. Electron Devices **54**, 2137 (2007).

[5] X. J. Yang, T. Kiba, T. Yamamura, J. Takayama, A. Subagyo, K. Sueoka, and A. Murayama, Appl. Phys. Lett. **104**, 012406 (2014).

[6] K. Takeishi, S. Hiura, J. Takayama, K. Itabashi, M. Urabe, A. Washida, T. Kiba, and A. Murayama, Phys. Rev. Appl. **10**, 034015 (2018).

[7] B. Pal, S. Y. Verbin, I. V. Ignatiev, M. Ikezawa, and Y. Masumoto, Phys. Rev. B **75**, 125322 (2007).

[8] A. Shabaev, E. A. Stinaff, A. S. Bracker, D. Gammon, and A. L. Efros, Phys. Rev. B **79**, 035322 (2009).

[9] H. Chen, S. Hiura, J. Takayama, S. Park, K. Sueoka, and A. Murayama, Appl. Phys. Lett., **114**, 133101 (2019).

[10] S. Park, H. Chen, S. Hiura, J. Takayama, K. Sueoka, and A. Murayama, ACS Omega **6**, 12, 8561 (2021).

[11] S. Sato, S. Hiura, J. Takayama, and A. Murayama, Appl. Phys. Lett. **116**, 182401 (2020).

[12] S. Park, S. Hiura, J. Takayama, K. Sueoka, and A. Murayama, Adv. Electron. Mater. **8**, 2200588 (2022).

[13] H. Chen, S. Hiura, J. Takayama, S. Park, K. Sueoka, and A. Murayama, Appl. Phys. Express **13**, 015003 (2020).

Chapter 3. Experimental Procedures

3.1 Device fabrication

Semiconductor-based optically active layers were grown on surfaces of GaAs wafer substrates by molecular beam epitaxy (MBE), and these sample growth and structures are described in the latter sections depending on the types of semiconductor nanostructure. After those sample growth, electric-field-effect optical spin devices were fabricated by following processes, as shown in Figure 3-1.

1) The semiconductor sample layers on GaAs substrates were cleaned using organic solvent such as acetone and isopropyl alcohol (IPA) to remove impurities and contaminations on the substrate.

2) Titanium (Ti) or Iron (Fe) base layer was deposited by electron-beam (EB) evaporation on the above semiconductor surface. On a Fe base layer, gold (Au) cover layer was formed to prevent oxidation of the Fe layer via resistive thermal evaporation.

3) Photoresists (PRs) were coated with a rotational speed of 5000 rpm using a spin coater machine, and then the sample was baked on a hot plate. The used PRs were LOR-1A and OFPR 800LR 34cp.

4) The PRs in response to light passing through the mask were removed via photolithography and development using NMD3.

5) Ti/Au electrodes were deposited by EB and resistive thermal evaporation, respectively. And then it removes all remaining PRs through lift-off with N, N-Dimethylaminoethyl methacrylate.

6) To etch a vertical trench, 2nd PR spin coating and photolithography were performed with different mask for etching.

7) Vertical trenches were formed by dry or wet etching. The Ti base layer was etched by reactive ion etching with Argon plasma, whereas the Fe base and Au cover layer were etched by wet etching using etchent

AURUM-304 and hydrochloric acid.

8) After lift-off, the device and pitch conversion board (PCB) were attached on copper plate. Finally, they were connected by wire bonding.

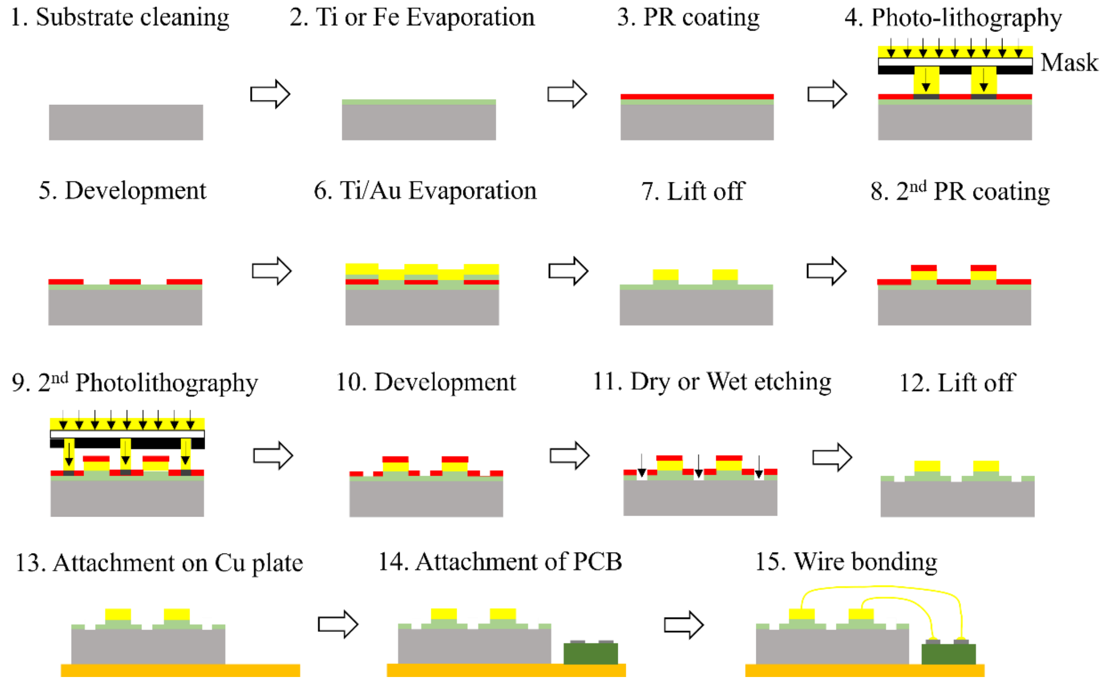

Figure 3-1 Schematic drawing of fabrication processes for electric-field-effect optical spin devices using semiconductor-based optically active layers.

3.2 Circularly polarized photoluminescence measurement

A schematic illustration of circularly polarized PL measurement is shown in Figure 3-2. Circularly polarized PL was detected by a cooled InGaAs detector through a spectrometer. A wavelength tunable pulsed laser with a repetition rate of 80 MHz and a pulse width of less than 120 fs was used as the excitation source, and it is passed through a combination of the $\lambda/4$ plate with a linear polarizer to convert into the circularly polarized light. The photon energy of the laser was tuned to 1.55 eV (800 nm) corresponding to the band gap of the GaAs barrier. Spin-polarized carriers generated at the GaAs barrier are entered into QW and then they are rapidly injected via spin-conserving tunneling into

the QDs. Circularly polarized PL emission from the QDs is condensed using an objective lens having 0.35 aperture and 20x magnification. A spectroscope and a CCD detector using a diffraction grating are used for detecting PL spectra. The degree of circular polarization of the PL is defined as circular polarization degree (CPD), as follows:

$$\mathrm{CPD}\ [\%] = \frac{(\mathrm{I_P} - \mathrm{I_{AP}})}{(\mathrm{I_P} + \mathrm{I_{AP}})} \times 100. \qquad (3\text{-}1)$$

Here, $\mathrm{I_P}$ and $\mathrm{I_{AP}}$ indicate PL intensities including spin-parallel (P) and anti-parallel (AP) electrons, respectively. In other words, they are defined as co- and cross circularly polarized PL against the orientation of excitation light. This CPD value reflects the electron spin polarization according to the equation (1-9).

To measure the time-resolved circularly polarized PL (TRPL), a mode-locked Ti:Sapphire pulsed laser with a repetition frequency of 80 MHz and a temporal width of less than 100 fs was used as the excitation source with a streak camera combined with a spectrometer. The full width at half maximum of the laser-pulse time response curve was 10 ps.

Furthermore, helium gas is supplied into a cryostat to which the sample is attached for measurement at low temperatures. Bias dependence is measured by applying a voltage with various ranges along the growth direction of the sample.

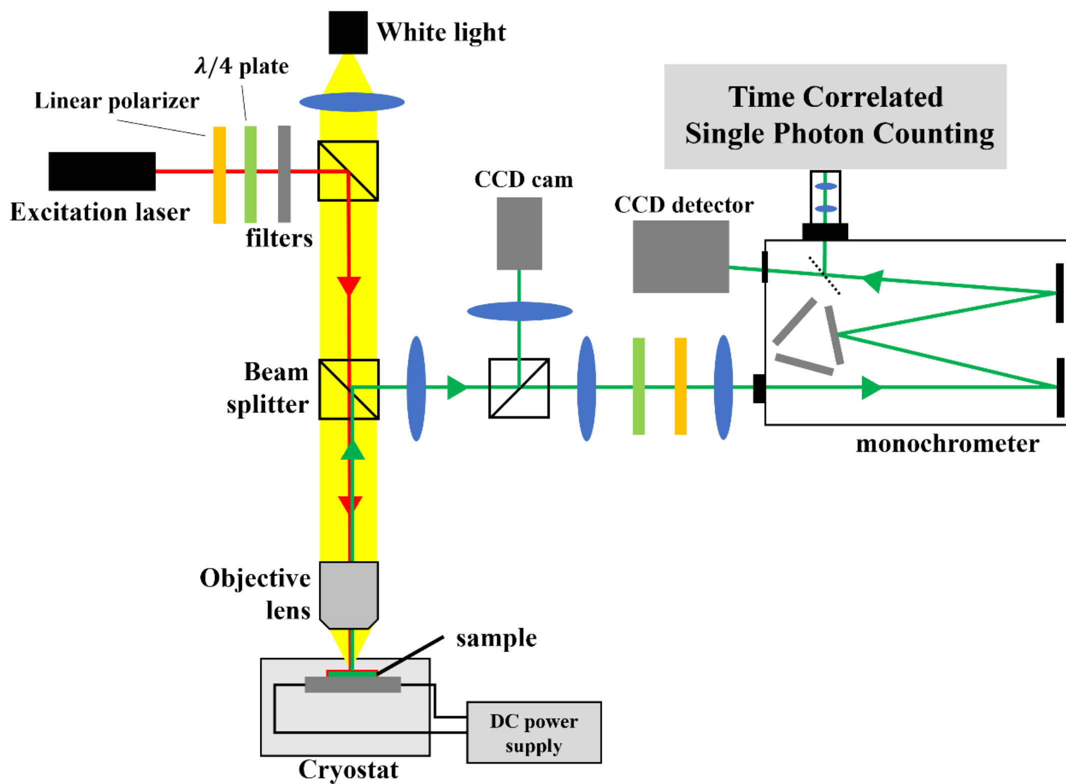

Figure 3-2 Schematic illustration of circularly polarized PL measurement using an optical microscope set-up.

Chapter 4. Temperature dependence of spin polarization with electric field in InGaAs QW/QD coupled structures

4.1 Background

I have fabricated electric-field-effect optical spin devices using InGaAs QW/QD coupled nanostructures and investigated the device performances at low temperatures [1, 2]. As a result, polarity and polarization degree of electron spin clearly depend on an external electric field since the number ratio of spin-polarized electron to hole injected into the QDs can be controlled by the applied bias voltage. However, the room temperature (RT) operation of the device is indispensable for practical applications. In this study, I investigate the temperature dependences of QD-PL and the corresponding CPD as a function of bias using the temperature-dependent circularly polarized PL measurements. I also conducted circularly polarized time-resolved PL measurements to figure out electron-spin dynamics up to RT [3].

4.2 Experimental procedures

Figure 4-1(a) shows a schematic drawing of the electric-field-effect optical spin device structure. The sample growth was conducted on p-doped GaAs (100) substrate along the z-direction by molecular beam epitaxy. A 20-nm-thick $In_{0.1}Ga_{0.9}As$ QW and $In_{0.4}Ga_{0.6}As$ QD layers as optically active layers were tunnel-coupled with an 8-nm thick GaAs tunneling barrier. The QD layer had relatively low surface density of $1.9 \times 10^{10}\ \mathrm{cm}^{-2}$. To apply an electric field, the sample was attached on a Cu plate, and a Ti/Au electrode was fabricated at a top of optical device. One side of the optical window provided on the electrode is about 20 μm. Two $Al_{1-x}Ga_xAs$ barrier layers were grown on the top and bottom of optically active layer to prevent external carrier injection from an

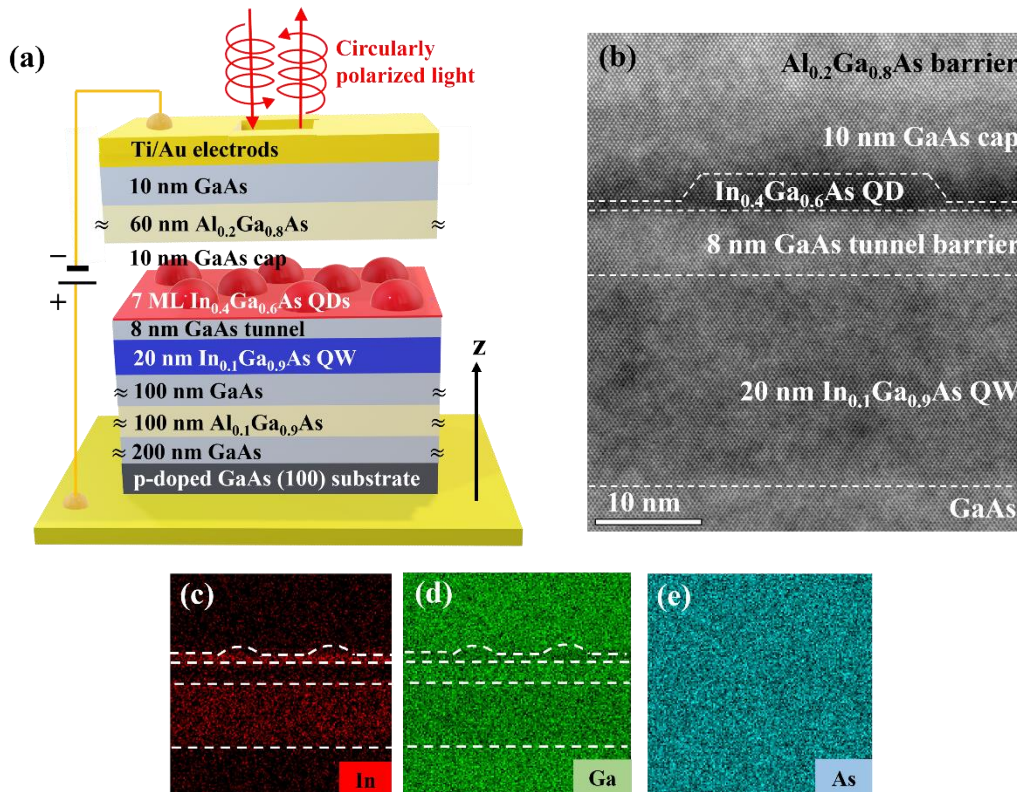

Figure 4-1 (a) Schematic illustration of a QW-QD tunnel coupled nanostructures-based optical device using electric field effect. (b) Cross-sectional HAADF STEM images and quantitative elemental maps of (c) In, (d) Ga and (e) As in the QW-QD coupled nanostructure by EDX.

electrode. The High-angle annular dark-field scanning transmission electron microscopy (HAADF STEM) image and quantitative elemental maps of In, Ga and As obtained by energy-dispersive x-ray (EDX) analysis are shown in Figure 4-1 (b)~(e), respectively. The observed QD has a diameter and a height of 25 and 4 nm. The In and Ga distribution are found by quantitative difference of atoms, however, As is not confirmed as shown in Fig. 4-1(e). The optically spin-polarized electrons are generated at 100 nm GaAs barrier under σ^--excitation laser with 800 nm wavelength. Excitation power of 0.2 mW was selected to suppress state-filling effect in the QDs. Electric field was applied along the z-direction and a range of applied bias voltages was –0.5~1.5 V, where the sufficient PL intensity can be obtained from the QD.

4.3 Bias dependence of electron-spin polarization at 4 K

At 4 K, QD-PL spectra and the corresponding CPD with bias voltages of 0.3 and 0.6 V are shown in Figure 4-2, respectively. The PL intensity peak at 1.26 eV corresponds to the energy-band gap between conduction and valence bands at the QD-GS, taking quantum confinement into account. The PL intensity is nearly constant at both 0.3 and 0.6 V. However, PL polarity and circular polarization show obvious differences between two bias conditions. At 0.3 V, a high negative CPD of about −20 % is observed at the QD-GS, as shown in Fig. 4-2 (a). In this condition, the coupled QW/QD potential tilts slightly toward the QD side, where excess spin-polarized electrons are injected into the QDs. Therefore, the spin-flip scattering at the QD-ES is enhanced due to the residual electron at the QD-GS, leading to the increased cross-circular PL against for the

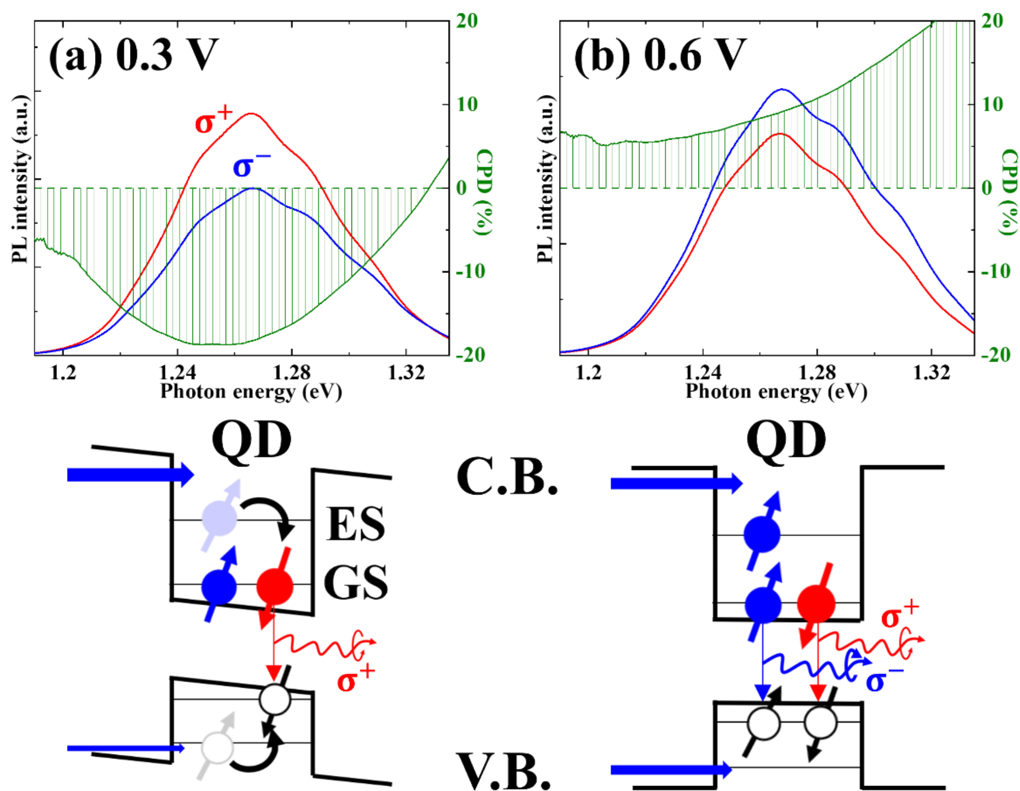

Figure 4-2 Circularly polarized PL spectra and the corresponding CPD with bias voltages of (a) 0.3 and (b) 0.6 V at 4 K. Schematic illustrations of each potential and the possible dynamics of spin-polarized carriers are shown below.

initial polarization of excitation. By contrast, the negative CPD disappears and positive CPD of about 8 % is observed at the QD-GS at 0.6 V. This is because the QW-QD potential is close to flat around 0.5 V, and then the hole injection is enhanced leading to the co-circular PL increases. As a result, it is found that CPD polarity can be changed by electric field even though the number of carriers emitted from the QDs is almost same.

Figure 4-3 shows a bias dependence of PL intensity and CPD at the QD-GS. Here, the QD-GS is defined as an energy range of 1.24~1.28 eV taking the inhomogeneous distribution of the QD size into account. The PL intensity peak is observed at 0.4 V, which is the best condition for the efficient tunnel injection of electron and hole into the QDs. However, the CPD at this bias condition is almost zero. It is guessed that the PL decay time is quite long (1.22 ns) in proportional to PL intensity, as following equation [3, 4]:

$$\mathrm{P_e} = \frac{\mathrm{P_0}}{(1 + \tau_{\mathrm{PL}}/\tau_{\mathrm{s}})}. \quad (4\text{-}1)$$

Here, $\mathrm{P_e}$ and $\mathrm{P_0}$ mean the electron-spin polarization degree and initial polarization in the QDs. τ_{PL} and τ_{s} denote the PL decay time and electron-spin relaxation time, respectively. But it is difficult to apply this equation to the calculation of negative spin polarization. Below 0 V, CPD value is nearly zero due to the suppressed hole injection into the QDs. The QW-QD potential considerably tilts toward the QW side, therefore, holes are localized in the QW leading to significant decrease in PL intensity. In this case, the spin polarization of electron in the QD can be depolarized while waiting for the injection of holes with parallel spin polarization, resulting in zero initial spin polarization in the QD-PL time profiles. Negative CPD is observed around 0.3 V, where the spin-flip scattering is enhanced due to the accelerated electron spin injection. In

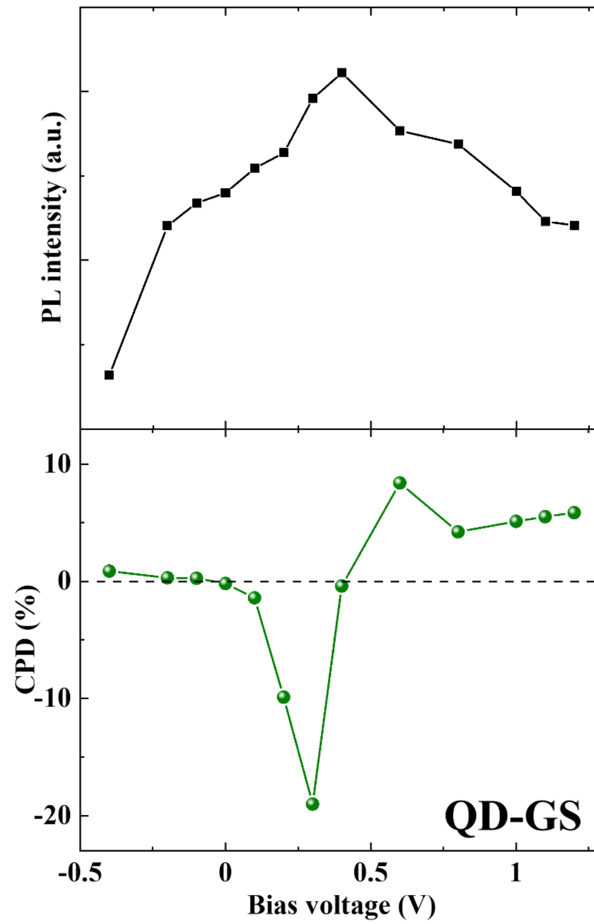

Figure 4-3 Bias dependence of PL intensity (above) and CPD (below) at the QD-GS.

these bias conditions, PL intensity with the negative CPD starts to drop. Since the effective mass of hole is heavier than that of electron [5], the hole tunneling rate from the QW to the QDs can be significantly affected by the shape and size distributions of the QD ensemble. Therefore, the number of QD satisfying a specific condition that the number ratio of electron to hole is 2:1 at the QD-GS is limited. Above 0.5 V, hole injection into the QD is accelerated, therefore, the negative CPD is disappeared. However, the potential tilted toward QW causes the reduction of electron injection into the QD, thus PL intensity starts to decrease as positive bias increases. As a result, the numbers of electron and hole injected into the QD can be precisely controlled by electric field at 4 K, as in the previous study [2].

Figure 4-4 shows time dependences of circularly polarized PL and the

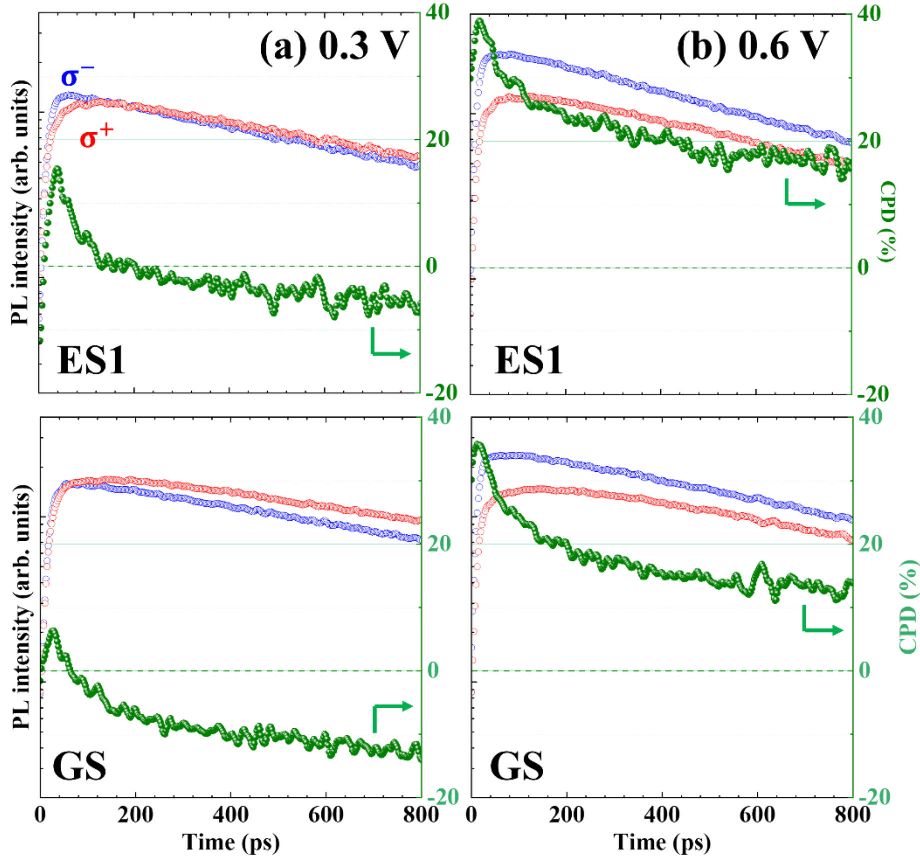

Figure 4-4 Circularly polarized time-resolved PL and the resultant CPD (upper panels) with a bias voltage of (a) 0.3 and (b) 0.6 V at the QD-GS (left panels) and ES1 (right panels) for 4 K.

corresponding CPD with bias voltages of (a) 0.3 and (b) 0.6 V at the QD-GS. The CPD decaying properties at the QD-ES indicate the spin-flip dynamics via electron-hole scattering. At 0.3 V, the negative CPD of the QD-ES is observed at 200 ps. The spin-flip dynamics become dominant at even the ES, and it is suggested that spin-flip scattering occurs at a higher state than the ES. The spin-flipped electron at the ES is rapidly energy-relaxed into the GS, therefore it starts to show the negative CPD of the GS at 60 ps. The significant CPD polarity change from 6 % to maximum degree of –12 % after 800 ps is observed at the QD-GS. In constant, initial positive CPDs up to 35 % at the GS decrease shapely down to 10 % at 800 ps owing to the spin relaxation, not involving the spin-flip scattering at 0.6 V.

4.4 Temperature dependence of electron-spin polarization

To find a temperature at which the negative CPD disappears, I study the temperature dependence of electron spin polarization. Figure 4-5 indicates circularly polarized PL spectra and the corresponding CPD with a bias voltage of 0.3 V at 40, 100, 180 and 250 K. The photon energy of the PL spectral peak corresponds to the PL emission from the QD-GS. Several weak PL peaks above the energy of the QD-GS is equivalent to the energy of some ESs. With increasing temperature, the peak energy of the QD-PL emission at both the GS and ES becomes lower due to the decreased number of carriers within the QD. The QD-GS transition energy of 1.26 eV at 40 K transfers to 1.19 eV at 250 K. This is due to the decreased band gap of QDs with temperature, following Varshni' law [7].

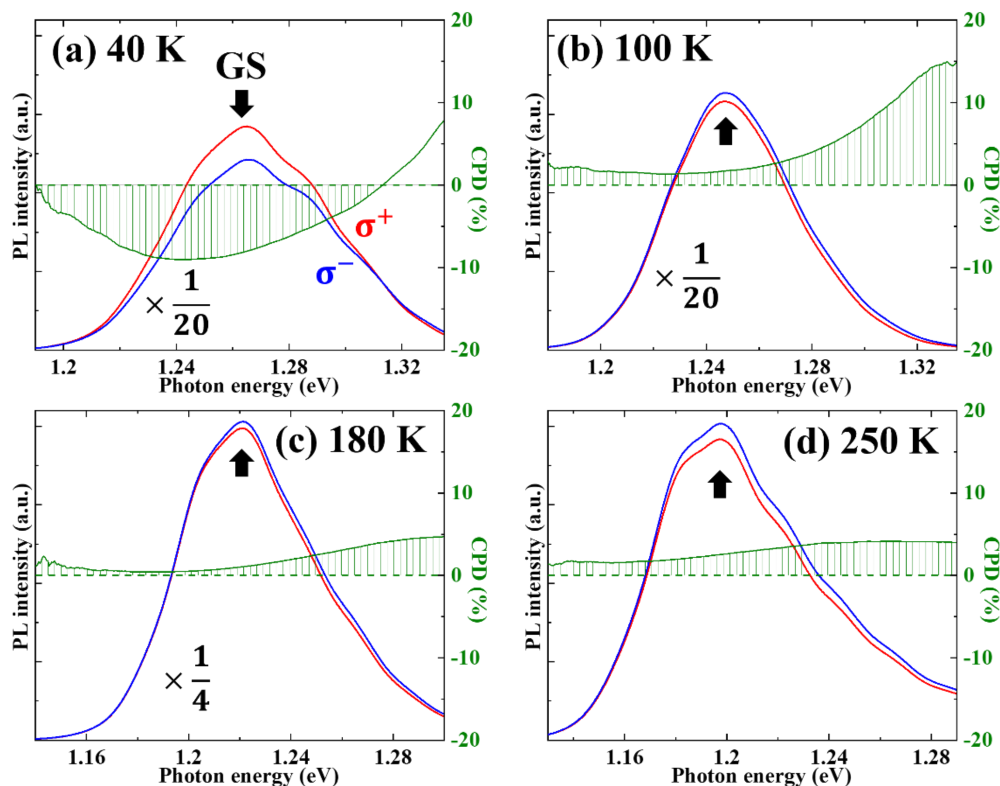

Figure 4-5 Circularly polarized PL spectra and the corresponding CPD with bias voltages of 0.3 V at (a) 40, (b) 100, (c) 180 and (d) 250 K.

$$E(T) = E(0) - \frac{\alpha T^2}{T + \beta} \qquad (4\text{-}2)$$

Here, $E(T)$ is the band gap at T °C, and α and β are constants. At 40 K, a negative CPD value of −8 % is observed at the QD-GS. The PL with negative CPD values originating from the spin-flipped electrons in the QD ensemble is still dominant at 40 K. However, this negative CPD value decreases compared to that at 4 K due to the enhanced spin relaxation originated from the acoustic phonon emission in the QD [6]. Despite the similar PL intensity, the negative CPD polarity is disappeared above 100 K because of the dissipation of residual electron by thermal escape from the QD-GS. At 180 and 250 K, The PL intensity decreases significantly by a factor of 5 or 20, respectively. In these temperatures, carriers start to escape out of the QDs. Rejection of spin-polarized electrons after thermal escaped does not cause significant change in CPD value. Figure 4-6 indicates the bias dependence of normalized PL intensity at 40, 100, 180 and 250 K. The PL line width as a function of

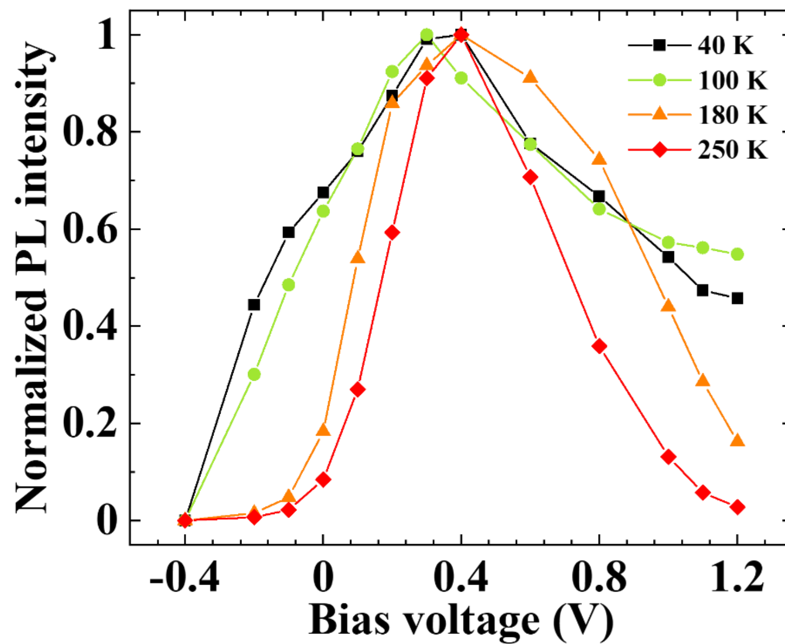

Figure 4-6 Bias dependences of normalized PL intensity with temperatures of 40, 100, 180 and 250 K.

bias voltages decreases above 100 K. This means that carriers tend to thermally escape out of the QDs owing to the potential modification by an electric field. In other words, it is suggested that the thermal escape rate of carriers strongly depends on applied bias voltage as increasing temperature.

Temperature dependences of PL intensity and CPD at the QD-GS is shown in Figure 4-7, and the inset in Fig. 4-7(a) indicates the PL decay time as a function of temperature at 0.3 V. The PL intensity is constant to 140 K since carriers excited to the ES with relatively small thermal energy can be rapidly relaxed into the GS. However, it starts to decrease sharply from 180 K due to thermal escape of carriers from the QDs. The

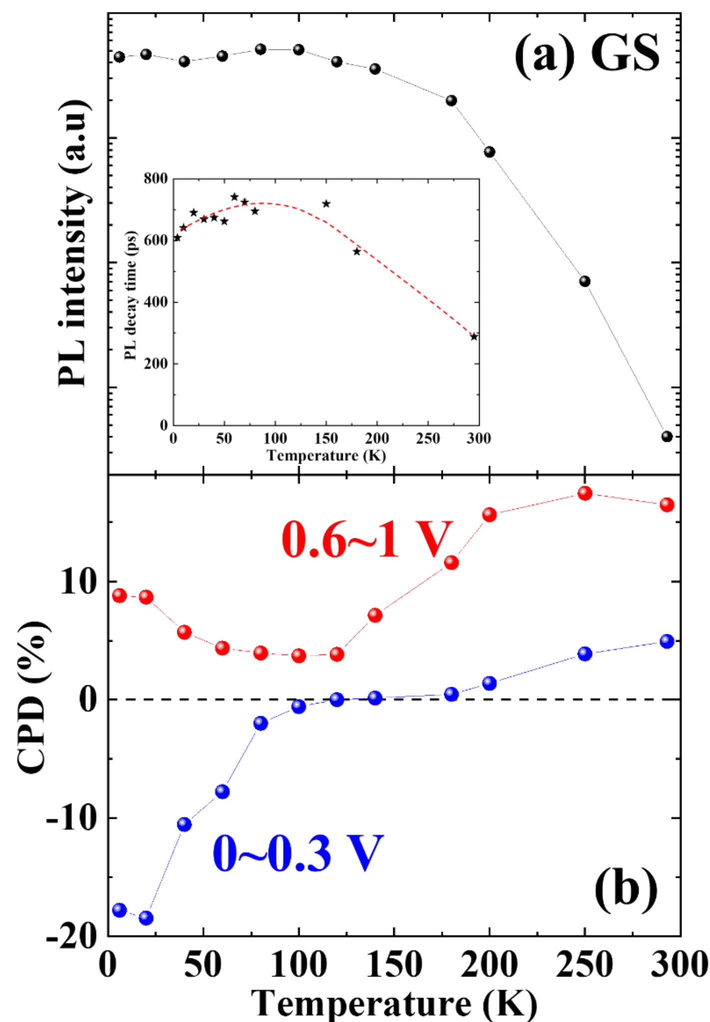

Figure 4-7 Temperature dependence of (a) PL intensity and (b) CPD at the QD-GS. The inset in (a) indicates the PL decay time as a function of temperature at 0.3 V.

temperature dependence of PL decay time shows the same trend as that of the PL intensity. It is observed that the PL decay time decreases from 700 ps below 100 K to 300 ps at 295 K. The temperature dependence of the CPD indicates a different trend depending on bias voltages, as shown in Fig. 4-7(b). First, positive CPD decreases from 4 to 100 K with bias voltages of 0.6~1 V. This can be attributed to the reduced spin relaxation time τ_s whereas PL decay time τ_{PL} is not changed remarkably, following the above equation (4-1). The electron-spin relaxation in the QDs is enhanced by emissions of acoustic phonons, corresponding to the thermal energy. From 120 K, the positive CPD increases gradually, owing to the significant reduction of PL decay time as the inset of Fig.4-7(a). Second, the negative CPD starts to decrease from 20 K, and it reaches to zero at 120 K. In these temperature conditions, the spin-flip mechanism of hole at the QD-ES can be enhanced by thermal energy when hole spin is energy-relaxed to the GS [8]. That is, the hole-spin state at the QD-GS can be flipped once again after this spin-flip scattering of electron-hole at the ES. As a result, co-circularly polarized PL increases in the QD ensemble, leading to the decline of negative CPD. Above 140 K, residual electrons at the QD-GS in the QD ensemble tend to be eliminated by thermal escape, and positive CPD increases due to the decreased PL decay time. Finally, it is found that CPD values at even 295 K is changed from 5 to 15 % by electric field. This result is discussed in more detail in the section 4.5.

The activation energy, responsible for the negative CPD, which can be calculated from the absolute value of CPD as a function of inverse of temperature is shown in Figure 4-8. As a result, the activation energy of 23 ± 5 meV is deduced, corresponding to the energy for the dissipation of negative PL polarization. This is similar with 22 meV of calculated energy difference between the QD-GS and the first excited state (ES1).

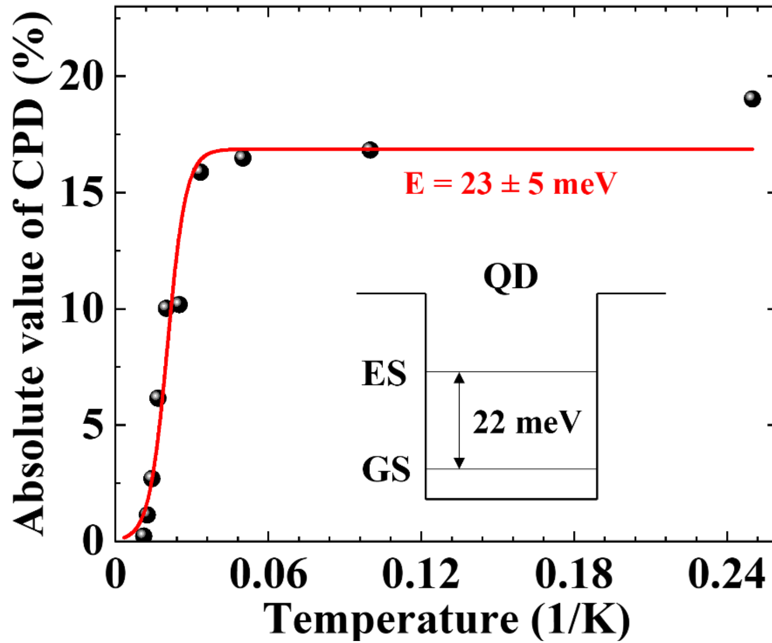

Figure 4-8 Activation energy calculated from the absolute value of PL polarization as a function of the reciprocal of temperature.

4.5 Electric-field control of electron-spin polarization at RT

Figure 4-9 (a) and (b) show PL intensity and the corresponding CPD at 1.1 and –0.1 V, respectively. These bias conditions were selected to compare the electric-field-effect on the electron-spin dynamics between the GS and ES with similar PL characteristics. The QD-GS and ES were defined with photon energy ranges of 1.16 ~ 1.20 eV and 1.22~ 1.26 eV, considering the QD size nonuniformity, respectively. The PL emission

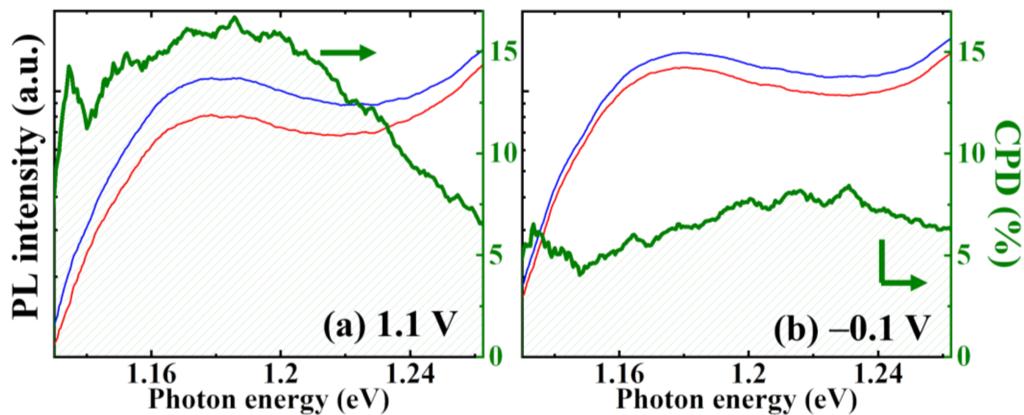

Figure 4-9 Spectra of PL intensity and the corresponding CPD with bias voltages of (a) 1.1 and (b) –0.1 V. The QD-GS and ES are defined with photon energy ranges of 1.16 ~ 1.20 eV and 1.22 ~ 1.26 eV, respectively.

above 1.26 eV is originated from a wetting layer (WL) of QD or QW. In the case of 1.1 V, a CPD value of 15 % is observed at the QD-GS, whereas it decreases to 5 % with bias voltage of –0.1 V. One can guess that this is because the spin-flip scattering remains with –0.1 V at even RT. In this bias condition, electron-spin injection is accelerated by tilted potential toward the QD side, and then a residual electron remains at the QD-GS. Therefore, the positive CPD value in the QD ensemble will decrease due to the spin-flip scattering, which resulted in emitting cross-circularly polarized PL. However, negative CPD is not observed at RT. It is suggested that the residual electron escapes from the QD-GS affecting by the thermal excitation, so emission of co-circularly polarized PL is still dominant in the QD ensemble. This is explored in more detail later in this chapter.

Figure 4-10 (a) shows PL-CPD of the QD-GS as a function of bias voltages, with various excitation conditions using different polarization

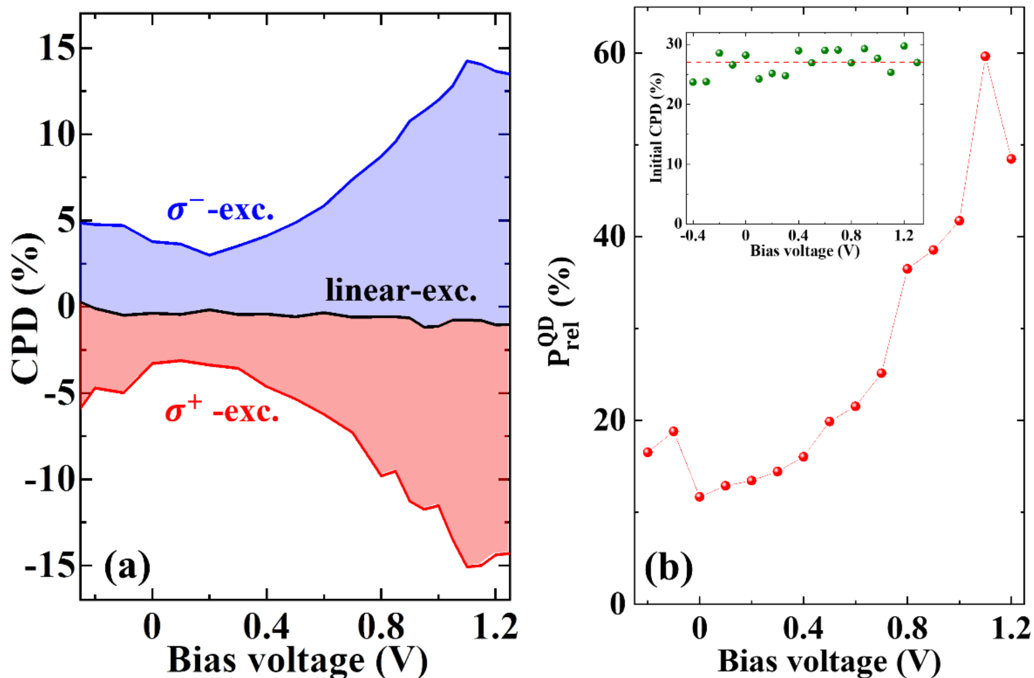

Figure 4-10 (a) CPD of the QD-GS as a function of bias voltage with different excitation polarization lights. (b) The ratio of initial CPD at the ES (see inset) and PL-CPD of the GS as a function of bias voltage.

lights. The CPD value is changed from minimum value of 3 % to maximum value of 15 % by applied bias voltages. This result shows that the spin polarization degree depends on the bias voltage at RT. There is no significant difference in CPD values regardless of co (σ^-)- and cross (σ^+) -circularly polarized excitation light. The linear excitation exhibits no polarization at all ranges of bias voltage. At low temperatures, CPD values can be switched more than 30 % in the section 4-3, in contrast, the control of spin polarization degree by electric field is weakened by thermal excitation at RT. The ratio of the degrees of PL polarization at the QD-GS to the initial spin polarization immediately after the spin-polarized electrons are injected into the QD-ES is shown in Fig. 4-10(b). This ratio is defined as P_{rel}^{QD} which value demonstrates spin-relaxation of electrons after injection from the QW into the QDs. The P_{rel}^{QD} is modified from 12 to 60 % by an electric field. The photo-excited electron-spin polarization in a GaAs bulk (barriers) is usually known to be 50 % according to the optical selection rule [9]. However, this polarization degree decreases in GaAs barriers or a QW before injection into the QDs owing to the DP mechanism, which is dominant at RT [10]. In fact, initial CPD values are not dependent on bias with 25-30 %, as shown in the inset of Fig. 4-10(b). This means that the degree of electron-spin relaxation before the injection into QDs does not change by the bias voltage. In addition, it implies that the QD-PL polarization is determined by electron-spin dynamics within the QD solely.

Transient PL and the corresponding CPD at the QD-GS and ES at 1.1 and –0.1 V are shown in Figure 4-11, respectively. The black solid line is the best fitted calculation of the CPD decay using a single-exponential decay fitting. The CPD decay time of a reference $In_{0.4}Ga_{0.6}As$ QD is 162 ps at the QD-GS. The obtained time constant of 146 ps at 1.1 V is close

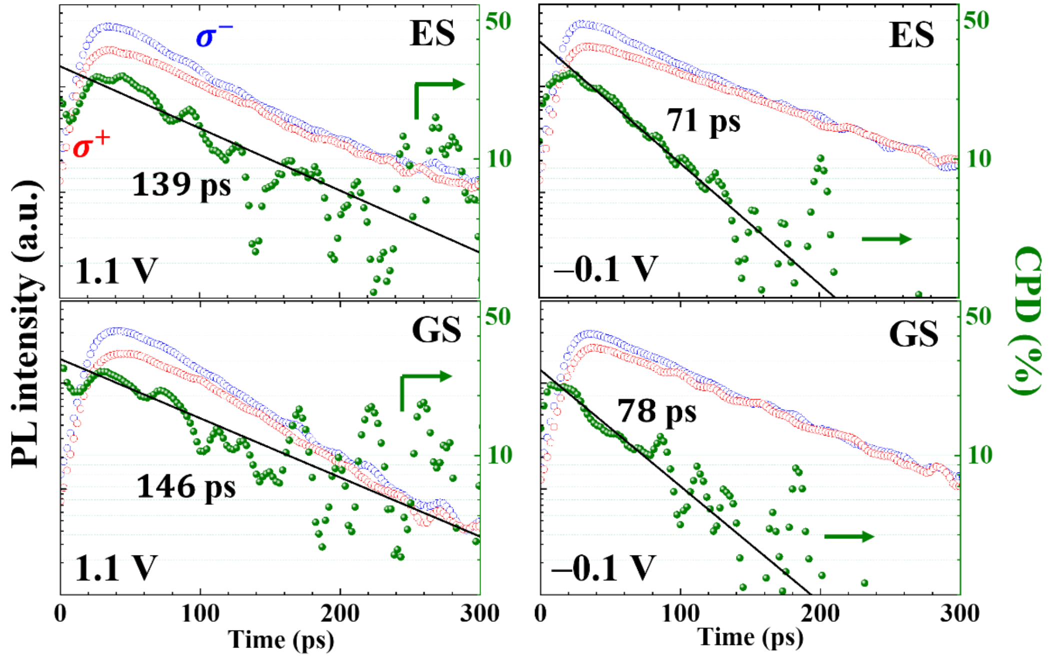

Figure 4-11 Time resolved PL spectra with bias voltages of (a) 1.1 and (b) -0.1 V at the QD ES (up) and GS (down). The black solid line is the best fitted calculation of CPD decay using rate equations.

to this value. However, 78 ps of the CPD decay time at −0.1 V is 2 times faster than that of 1.1 V. At low temperatures as described above, the negative PL polarization is observed at specific bias conditions, originating from the residual electron generated by the accelerated electron-spin injection into the QDs. This disappears due to the thermal escape of the residual electron with increasing temperature. However, large number of spin-polarized electrons injected into the QDs still occupy the QD-GS even at RT according to the Boltzmann distribution. That is, the residual electron may exist at the QD-GS when electron-spin injection is accelerated with specific bias condition. Here, I assume that low CPD and fast τ_s obtained below −0.1 V are originated from the spin-flip scattering remained even at RT.

To support my assumption, rate equation analysis for time-resolved PL is performed, which has been used to estimate spin-flip time based on a previous study [11]. Figure 4-12(a) shows the simulation results of transient PL polarization by difference in the spin-flip time $\tau_{sf} = \tau_{s1} -$

τ_{s2} with the fixed value of τ_{s2}=214 ps, which is deduced from a CPD decay time of the QD-ES for a reference $In_{0.4}Ga_{0.6}As$ QD. A schematic model of this asymmetric spin-flip with electron-spin relaxation time τ_{s1} and τ_{s2} is presented in the inset of Fig.4-12(e). In this model, blue up- and red down-spin indicate the majority and minority electron spins in the QDs, respectively. When τ_{s1} of the relaxation time from the majority into minority spins is faster than τ_{s2}, those difference is negative, as shown in Fig.4-12(a). According to these simulation results, high negative CPD with steep PL polarization decays are obtained as the negative value of τ_{sf} increases. It means that the spin-flip dynamics is dominant in the QD ensemble, resulting from the residual electron formed by the enhanced electron-spin injection into the QDs. In other words, the existence probability of the minority spins in the QD increases by faster switching time τ_{s1}, as a result, the PL emission with cross-circularly polarization also increases from the QDs. With the rate equation analysis, circularly polarized PL time profiles and the corresponding CPD of the QD-ES are shown at bias voltages of (b) 1.1, (c) 0.1, and (d) –0.1 V. The black solid lines indicate the best fitted results calculated by $\tau_{s1} - \tau_{s2}$. In the normal case without the spin-flip scattering, the fitted line decreases almost linearly like 1.1 and 0.1 V, showing the usual spin relaxation. In contrast, the curve of the fitted CPD graph falls rapidly into negative value at –0.1 V. This can be induced by faster τ_{s1} indicated the abovementioned spin-flip scattering. The $\tau_{s1} - \tau_{s2}$ has the bias dependence following the red broken line, as shown in Fig.4-12(e). Below 0.1 V, the spin-flip time decreases gradually and is

obtained with the value of –30 ps at –0.1 V. However, the spin-flip scattering for RT is suggested to be suppressed when compared to –65 ps obtained at low temperature. With increasing temperature, residual electron-spins at the QD-GS are likely excited thermally. As a result, the number of QDs in the ensemble, where the spin-flip scattering occurs, is limited, and then the PL emission intensity with cross-circular polarization decreases.

The PL decay time (τ_{PL}) and twice the CPD decay time ($2\tau_{CPD}$) as a function of bias voltage are shown in Figure 4-13(a) and (b), respectively. The bias dependence of τ_{PL} shows the same trend as that of the QD-PL intensity, and the peak of τ_{PL} with 264 ps is also observed at 0.3 V. This

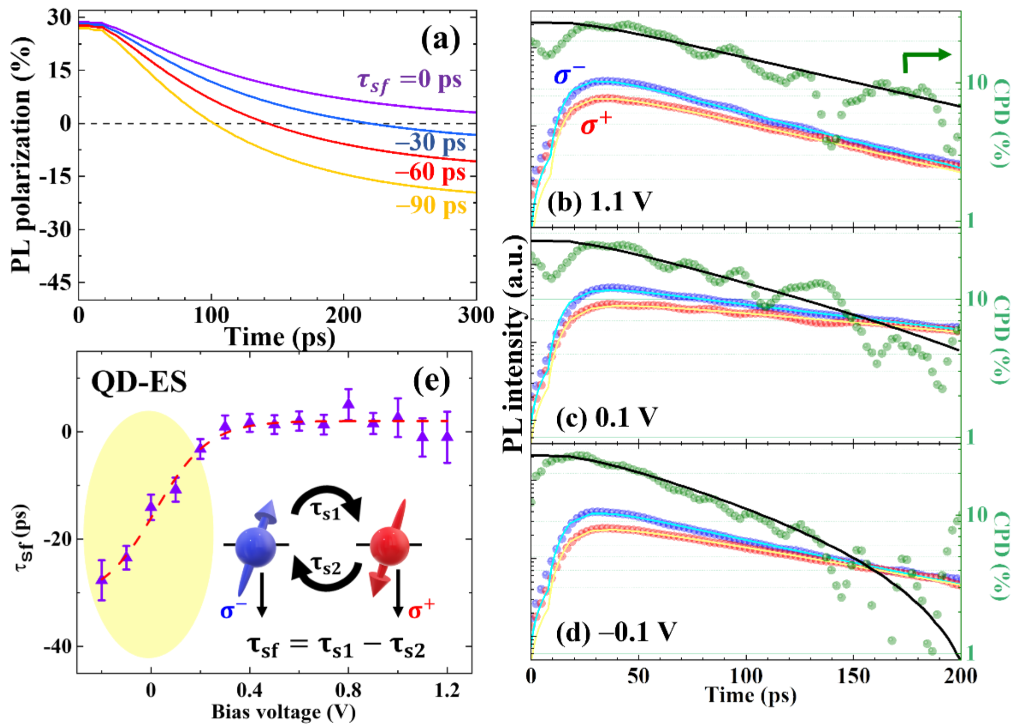

Figure 4-12. (a) Simulation results of transient CPD at the ES with various spin-flip time τ_{sf}=τ_{s1}-τ_{s2} and fixed value of τ_{s2} = 246 ps. Circularly polarized PL time profiles and corresponding CPD of the ES at bias voltages of (b) 1.1, (c) 0.1, and (d) –0.1 V. The black solid lines indicate the best fitted results. (e) Bias dependence of τ_{sf} at the ES. The red broken line is a guide for the eyes. The inset shows a schematic model of asymmetric spin-flip dynamics with electron-spin relaxation times of τ_{s1} and τ_{s2}. In this model, blue up-spin and red down-spin mean the majority and minority electron spins in QDs, respectively.

voltage is the best condition that electrons and holes are efficiently injected into the QDs, where it satisfies their number ratio of 1:1 within the QDs. However, it should be noted that this condition is not suitable for the efficient spin-photon conversion due to the similar value between τ_{PL} and $2\tau_{CPD}$, as shown in Fig.4-13(a). When the τ_{PL} is less than 50 ps, the PL emission from the QD is very weak due to the strong potential modification that interrupts the injection of electrons or holes into the QD. The value of $2\tau_{CPD}$ also depends on the applied bias voltage with the red broken guideline. Below 0.3 V, the $2\tau_{CPD}$ starts to decrease gradually, and it indicates the similar trend as that of τ_{sf}. $2\tau_{CPD}$ is defined by a function of electron-spin relaxation and spin-flip times. However, electron-spin relaxation time has no bias dependence in the

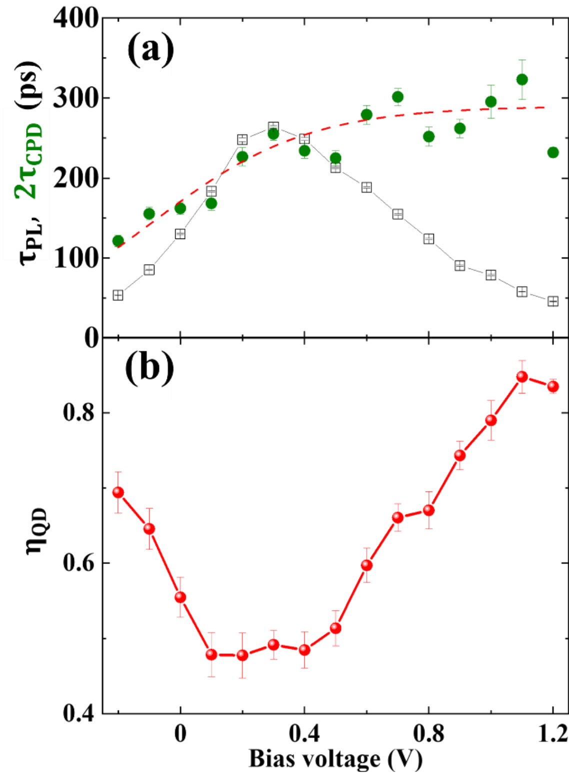

Figure 4-13 (a) Bias dependence of PL decay time τ_{PL} (open black squares) and twice the CPD decay time: $2\tau_{CPD}$ (green circles). The broken red line is a guideline for $2\tau_{CPD}$. (b) The photon/electron-spin conversion parameter η_{QD} as a function of bias voltage, which is calculated by τ_{PL} and $2\tau_{CPD}$.

QD. Therefore, this decline in the $2\tau_{CPD}$ with bias voltages can be related to the enhanced spin-flip scattering, as described above. The photon/electron-spin conversion parameter η_{QD} as a function of bias voltage is shown as Fig. 4-13(b), based on equation calculated by τ_{PL} and $2\tau_{CPD}$, as follows [4]:

$$\eta_{QD} = \frac{1}{1+\frac{\tau_{PL}}{2\tau_{CPD}}} \tag{4-3}$$

This parameter indicates the efficiency from electron-spin polarization into circular polarization of photon. The η_{QD} also strongly depends on bias voltage at RT, showing a similar trend as the bias dependence of P_{rel}^{QD}. The $2\tau_{CPD}$ (323 ps) at 1.1 V is 3 times longer than τ_{PL} (58 ps), therefore high η_{QD} of more than 0.8 is obtained. That is, the high PL polarization of 15 % at 1.1 V is mainly originated from this high η_{QD}. With decreased bias voltage, the value of η_{QD} drops greatly to 0.5 due to the increase in τ_{PL} with respect to almost constant τ_{s}. Below 0.1 V, PL emission is suppressed by slow hole injection into the QDs, and then it induces shorten τ_{PL}, resulting in the enhanced η_{QD}.

4.6 Conclusion

I have studied the temperature dependence of electric-field effect on the PL-CPD reflecting spin polarizations of photo-excited carriers using a conventional III-V compound semiconductor InGaAs-based QW-QD tunnel-coupled nanostructure. The CPD values are manipulated in the range of 3-15 % by an external bias application, corresponding to the 12-60 % change in the internal spin-polarization change: P_{rel}^{QD}. Despite RT,

I find that one can control the PL-CPD, i.e., spin polarization, by using electric field only.

In addition, spin-flip dynamics within the QDs is observed even at RT and can also be controlled by the electric field. This can greatly facilitate practical applications of semiconductor spintronics with the electric field manipulation of spin information.

The next task is, it is necessary to suppress the thermal escape of spin-polarized electrons from the QDs to improve room-temperature performances.

Bibliography

[1] H. Chen, S. Hiura, J. Takayama, S. Park, K. Sueoka, and A. Murayama, Appl. Phys. Lett., **114**, 133101 (2019).

[2] S. Park, H. Chen, S. Hiura, J. Takayama, K. Sueoka, and A. Murayama, ACS Omega **6**, 12, 8561 (2021).

[3] S. Park, S. Hiura, J. Takayama, K. Sueoka, and A. Murayama, Adv. Electron. Mater. **8**, 2200588 (2022).

[4] S. Hiura, M. Takishita, J. Takayama, S. Sato, and A. Murayama, Phys. Rev. Appl. **14**, 044011 (2020).

[5] A. P. Zhou and W. D. Sheng, Eur. Phys. J. B **68**, 233 (2009).

[6] A. Tackeuchi, R. Ohtsubo, K. Yamaguchi, M. Murayama, T. Kitamura, T. Kuroda and T. Takagahara, Appl. Phys. Lett. **84**, 3576 (2004).

[7] Y. P. Varshni, Physica **34**, 154 (1967).

[8] I. V. Ignatiev, S. Y. Verbin, I. Y. Gerlovin, R. V. Cherbunin and Y. Masumoto, Optics and Spectroscopy **106**, 375 (2009).

[9] F. Meier and B. P. Zakharchenya, Optical orientation, Elsevier, North Holland (1984).

[10] M. I. D'yakonov and V. I. Perel', Sov. Phys. JETP **38**, 177 (1974).

[11] S. Hiura, S. Hatakeyama, J. Takayama, and A. Murayama, Appl. Phys. Lett. **116**, 262407 (2020).

Chapter 5. Electric-field-effect on spin polarization in InGaAs QW/InAs QD coupled structures

5.1 Background

I have studied bias and temperature dependences of electron-spin polarization for InGaAs QW/QD tunnel-coupled nanostructures, as described in the previous chapter. At RT, the PL polarization decreases, which can be affected by the thermally spin-depolarized electrons in the QDs. Therefore, it is necessary to suppress the thermal distribution of spin-polarized carriers for practical optical applications at RT.

In this study, I fabricated electric-field-effect optical spin device using InAs QDs coupled with InGaAs QWs. The InAs QD has an advantage that the energy difference between the QD-ES and GaAs barrier is significantly larger than the thermal energy. Therefore, I have investigated the bias and temperature dependences of the PL polarization in the InGaAs QW/InAs QD tunnel-coupled nanostructures.

5.2 Experimental procedures

Figure 5-1(a) shows a schematic drawing of the electric-field-effect optical spin device structure. The sample growth was conducted on a p-doped GaAs (100) substrate along the z-direction by molecular beam epitaxy. 20-nm-thick $In_{0.1}Ga_{0.9}As$ QW and p-doped InAs QD layers were tunnel-coupled with an 8-nm thick GaAs tunneling barrier. The QD layer had relatively low surface density of $2 \times 10^{10}\ \mathrm{cm}^{-2}$. Based on the previous study [1], the QD was doped with Be using remote doping for 4 holes/QD. To apply electric field, the sample was attached on a Cu plate, and a Fe/Au/Ti/Au electrode was fabricated at a top of optical device. To prevent the effects of iron on the PL properties, MgO barrier was deposited under the electrode. One side of the optical window provided

on the electrode is about 20 μm. Two $Al_{1-x}Ga_xAs$ barrier layers were grown on the top and bottom of optical active layer to prevent an external carrier injection from an electrode. A schematic potential of this structure is shown in Fig.5-1(b). The circularly polarized laser was set to 800 nm (1.55 eV) for the excitation in GaAs, and the laser power of 200 μW was selected to prevent the state-filling-effect in the QDs [5]. Spin-polarized electron and hole pairs are generated in GaAs barriers under σ^+-excitation, and then they are injected from the QW into the QDs via spin-conserved tunneling. The doped holes compensate for the absence of slow hole injection from the QW to the QDs. Finally, the electron-hole pairs recombine and disappear in the QDs, emitting circularly polarized PL depending on the spin states.

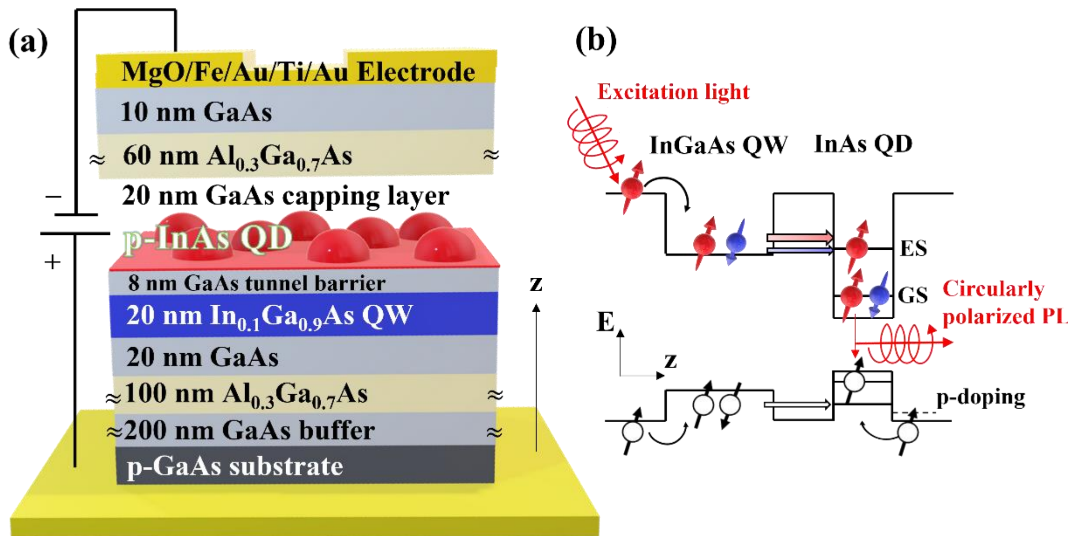

Figure 5-1 Schematic drawings of (a) electric-field-effect optical spin device using InGaAs QW/p-doped InAs QD coupled nanostructures and (b) the band potentials with a luminescent process reflecting the spin-polarized carrier dynamics in the coupled nanostructure.

5.3 Bias dependence of electron-spin polarization at 4 K

Figure 5-2 indicates PL spectra and the corresponding CPD with bias voltages of (a) –2, (b) 0.4 and (c) 2.4 V, respectively. The QD-PL intensity

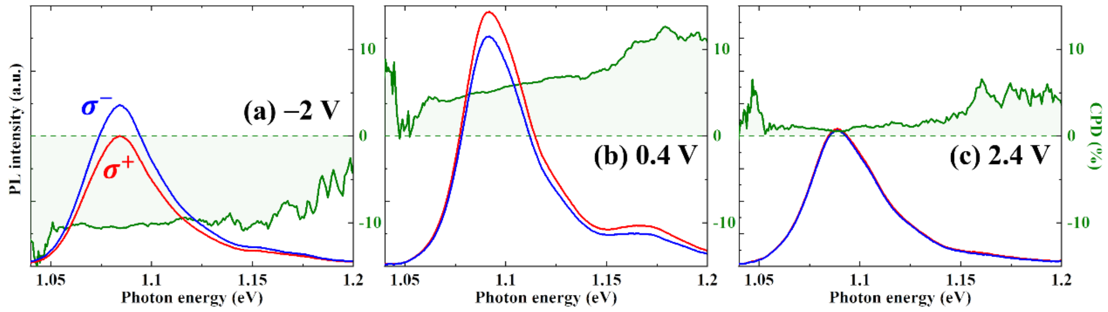

Figure 5-2 Circularly polarized PL spectra and the corresponding CPD with bias voltages of (a) −2, (b) 0.4 and (c) 2.4 V, respectively.

peaks at 1.08 eV, which corresponds to the light emission from the QD-GS. This peak energy of the QD-GS account for a characteristic of InAs QD as compared to 1.26 eV of the InGaAs QD in the section 4.3. The weak PL peak above 1.15 eV originates from the QD-ES. Lower PL intensity is obtained at –2 and 2.4 V, as compared to that at 0.4 V. The injection of hole and electron into the QDs can be suppressed by the potentials tilted toward the QD or QW side depending on bias, respectively. Negative CPD of −10 % at the QD-GS is obtained by the enhanced electron spin injection into the QDs at −2 V, as described above. This negative PL polarization disappears according to the elimination of residual electron at 0.4 V, indicating positive CPD of 5 %. At 2.4 V, no polarization of 0.5 % is observed whereas PL intensity is constant with that of −2 V.

The bias dependence of PL intensity and CPD at the QD-GS is shown in Figure 5-3(a) and (b). PL intensity profile as a function of bias voltage indicates the oscillation behaviors. This can be originated from longitudinal optical (LO)-phonon mediated resonant tunneling [2]. In the 2D-QW and 0D-QD coupled structure, it is known that electron wave function between the QW initial state and the QD-ES is strongly coupled via the wetting layer [3, 4], as shown in Fig.5-3(c). This electron wavefunction penetration becomes weaker or stronger depending on

electric-field conditions. If the energy difference between the initial state of the QW and one of the QD-ESs is equivalent to the resonant phonon energies E_{LO} with several LO-phonons, ultra-fast energy relaxation emitting LO-phonons can be induced as Fig.5-3(d). The 1LO phonon energy is about 36 meV in GaAs. At bias with the higher PL intensity as −3, −1 and 1 V, the energy difference between the QW and the QD-ES is equivalent to the energies of several LO-phonons. Due to LO-phonon-induced resonant tunneling, electrons with the majority spin state are efficiently injected into the QDs, therefore, negative CPD becomes weaken and positive CPD enhances. The negative CPD disappears when spin-flip scattering is suppressed above −1 V. Almost no polarization above 1 V can be attributed to the hole-state filling effect at the QD-GS.

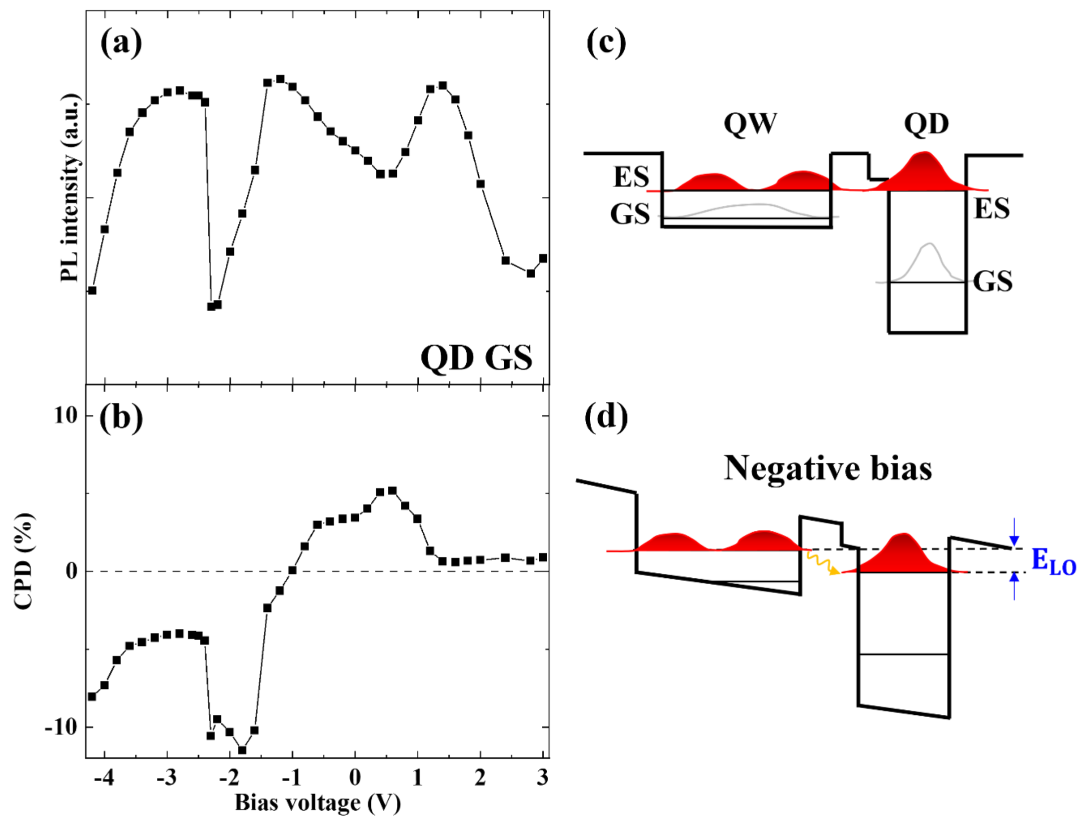

Figure 5-3 Bias dependence of (a) PL intensity and (b) CPD at the QD-GS. A schematic drawing of the electron wave function in the QW-QD coupled potential.

5.4 Temperature dependence of electron-spin polarization

Figure 5-4 shows contour plots of the QD-PL intensity at (a) 4, (b) 60, (c) 160 and (d) 225 K. The photon energy with the highest PL peak is shifted to the lower side with increasing temperatures, following Varshni' law in equation (4-2). The strong PL intensity oscillation by LO-phonon mediated resonant tunneling is observed at both 4 and 60 K. On the other hand, the oscillation behavior is vanished at 160 and 225 K. The PL peak is only observed around -1 V, which is the best condition for the efficient tunnel injection of electrons and doped holes into the QDs. One can guess that the concubine of PL intensity oscillation is originated from the weaken wavefunction penetration of electrons due to thermal energy. Carriers can be thermally escaped from the QDs as well as the QW at high temperatures. This thermal escape probability of carriers from the

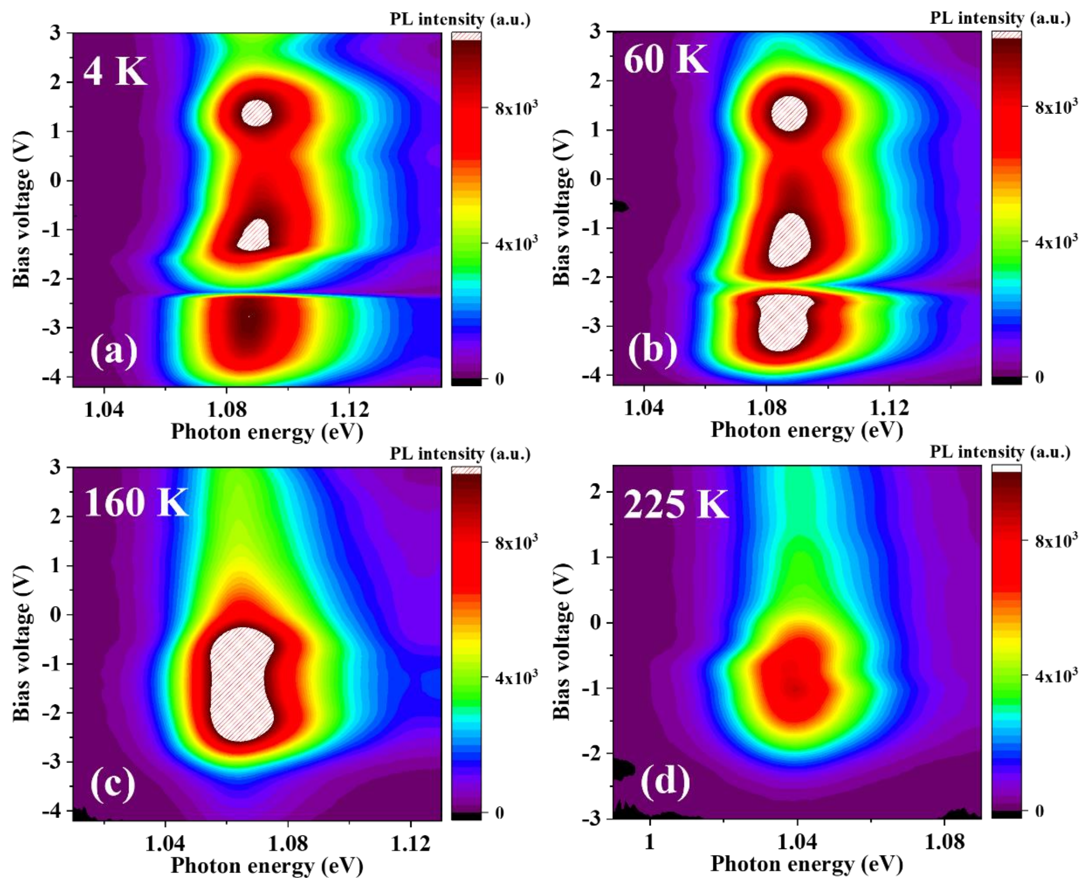

Figure 5-4 Contour plots of the QD-PL intensity at (a) 4, (b) 60, (c) 160 and (d) 225 K. The peak of PL intensity is observed at -1 V.

QDs strongly depends on electric field due to the strong potential modification, as described above. In addition, with increasing temperatures, the voltage range at which PL intensity is observed is limited, as shown in Fig.5-4(d).

Temperature dependences of PL intensity and CPD with a bias voltage of −2 V at the QD-GS is shown in Figure 5-5. The PL intensity is constant up to 180 K, and this indicates the suppressed thermal escape of carriers, as compared to 140 K in InGaAs QW/QD [Fig.4-7]. Owing to the deep energy levels of the InAs QD, the escaped carriers to the QD-ES are rapidly energy-relaxed at the middle temperature range, leading to the high PL intensity. Above 180 K, the PL intensity starts to drop shapely

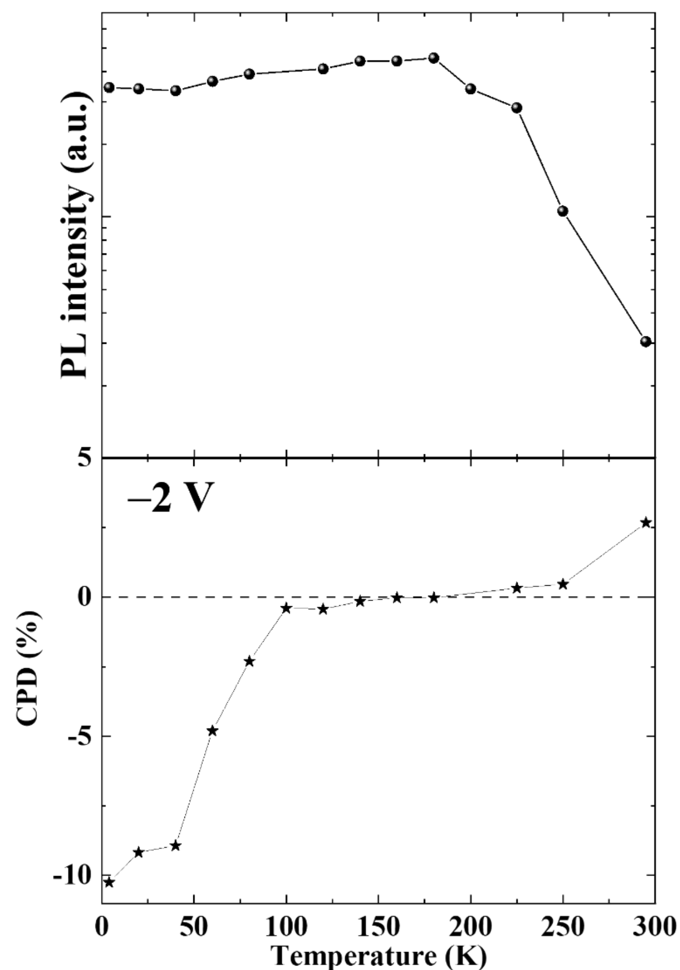

Figure 5-5 Temperature dependence of PL intensity (upper panel) and CPD (lower panel) with a bias voltage of −2 V at the QD-GS.

because of higher thermal energy. On the other hand, negative CPD of −10 % decreases gradually with increasing temperature, and it disappears at 160 K. This temperature, where negative PL polarization is dissipated, is higher than that in InGaAs QD (in the section 4.4). Therefore, the thermal escape of residual electron at the QD-GS is relatively suppressed in this sample. The increase of positive CPD above 180 K is originated from the fast PL decay times which corresponds to PL intensity, according to equation (4-1). However, entirely low CPD value is observed when compared to that in InGaAs QD. It is guessed that longer PL decay time than spin relaxation time lowers PL polarization.

5.5 Bias dependence of electron-spin polarization at RT

Figure 5-6 shows bias dependence of (a) PL intensity, (b) CPD, (c) PL decay time and (d) CPD decay time at the QD-ES for RT. The PL peak is observed on the negative voltage side due to the compensated hole

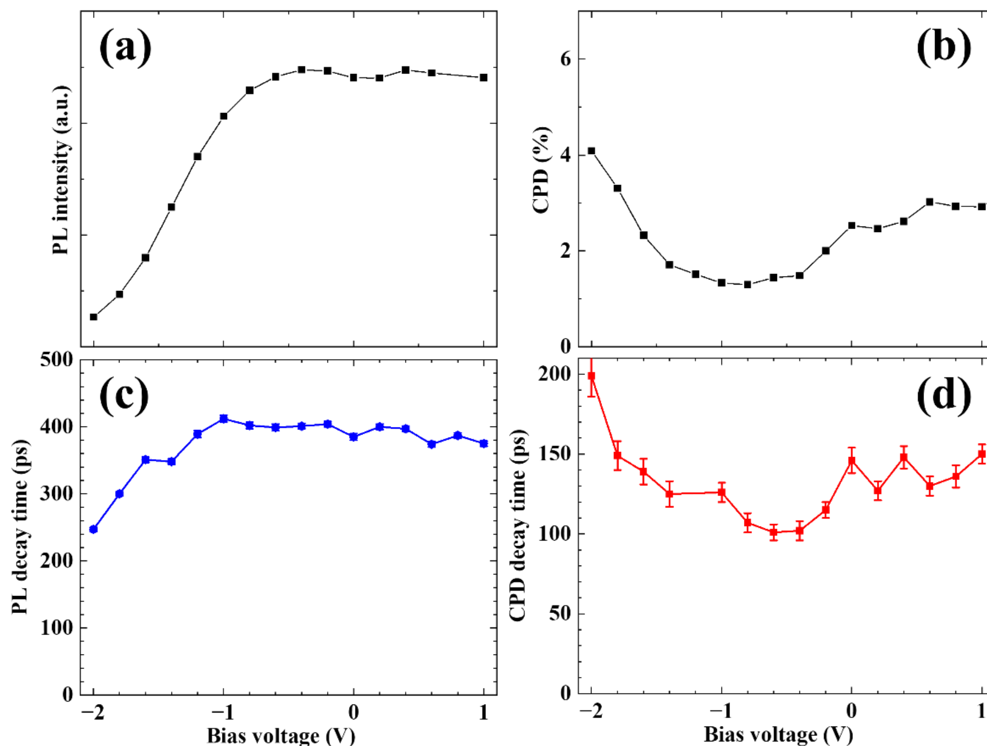

Figure 5-6 Bias dependences of (a) PL intensity, (b) CPD, (c) PL decay time and (d) CPD decay time at the QD-ES under RT.

injection by p-doping effect. The constant PL intensity above 0 V is originated by MgO. Below −1 V, PL intensity starts to decrease because of the absence of hole within the QDs. The PL decay time shows the same trend as that of the PL intensity. $\tau_{PL} = 412$ ps at −1 V decreases two times to $\tau_{PL} = 247$ ps at −2 V, leading to the decreased PL intensity. On the other hand, CPD value is markedly lower in the wide bias range. Faster CPD decay times than PL decay times in all bias range are responsible for the lower CPDs, while the initial CPD indicates no bias dependence with 60-67 %. The decrease of PL decay time results in slightly the enhanced CPD below −1 V.

5.6 Conclusion

I have studied the temperature dependence of the PL polarization in an electric-field-effect optical spin device using InGaAs QW-InAs QD coupled nanostructure. The oscillation of PL intensity by LO-phonon mediated resonant tunneling is observed at low temperatures. This promotes efficient injection of majority (parallel) spins into the QDs. This oscillation behavior disappears with increasing temperature, because of the thermal re-distribution of carriers.

The negative CPDs with anti-parallel spin polarization for the initially excited one disappears at 160 K. This result demonstrates the suppressed thermal escape of carriers from InAs QD, compared to the above case employing InGaAs QDs. The high PL intensity is obtained in the former InAs QDs at RT compared to the latter InGaAs ones, however, the PL-CPD values at RT is lower due to the longer PL decay time and faster spin relaxation time.

Bibliography

[1] S. Park, H. Chen, S. Hiura, J. Takayama, K. Sueoka, and A. Murayama, ACS Omega **6**, 12, 8561 (2021).

[2] H. Chen, S. Hiura, J. Takayama, S. Park, K. Sueoka, and A. Murayama, Appl. Phys. Express **13**, 015003 (2020).

[3] X. J. Yang, T. Kiba, T. Yamamura, J. Takayama, A. Subagyo, K. Sueoka, and A. Murayama, Appl. Phys. Lett. **104**, 012406 (2014).

[4] K. Takeishi, S. Hiura, J. Takayama, K. Itabashi, M. Urabe, A. Washida, T. Kiba, and A. Murayama, Phys. Rev. Appl. **10**, 034015 (2018).

[5] S. L. Chen, T. Kiba, X. J. Yang, J. Takayama, and A. Murayama, Appl. Phys. Lett. **108**, 152103 (2016).

Chapter 6. Electric-field-effect on spin polarization in GaNAs QW/InAs QD

6.1 Background

To realize fiber-optic communication systems, the wavelength of the emitted light should be between 1.3 to 1.55 μm. However, III-V semiconductor In(Ga)As QDs have an emission wavelength of 1.3 μm or less [1]. To overcome this limitation, InAs QD structures coupled with GaNAs strain-compensating layers (SCLs) are introduced. The band gap energy of InAs QD is reduced because the GaNAs SCLs alleviate the compressive strain in InAs QD. This causes the PL peak shift toward longer wavelength [2]. Furthermore, it is recently reported that high electron spin polarization of 90 % can be achieved in InAs QD-diluted nitride GaNAs coupled structure at RT [3]. The spin-filtering effect is responsible for this extremely high value of spin polarization at RT, where the minority electron spins can be selectively trapped by deep level defects within the GaNAs with small contents of N such as 1 %. In Ga-based compound semiconductors, Ga self-interstitials form spin-polarized defects acting as spin filtering sources [4-6]. The energy levels of the defects in the GaNAs are located deeper than thermal activation energy at RT, that spin filtering effect for the conduction electrons can work efficiently before spin injection into the QDs against for the thermal effect at RT.

In this study, for high PL polarization reflecting electron spin polarization at RT, I have fabricated electric-field-effect optical spin devices using 5 nm-thick GaNAs QW/InAs QD tunnel-coupled nanostructures and demonstrate bias dependence of the PL polarization at 4 and 295 K.

6.2 Experimental procedures

Figure 6-1(a) shows a schematic drawing of electric-field-effect optical spin device using GaNAs QW-InAs QD coupled nanostructure. A 5 nm-thick-GaNAs QW and a single InAs QD layer was coupled with 3 nm-thick-GaAs tunneling barrier. They were grown on a Zn doped GaAs (100) substrate via molecular beam epitaxy (MBE). The nitrogen composition of GaNAs QW is set to 0.9 %. A QW/QD coupled optically active layer was capped 10 nm-thick-GaAs. Two $Al_{0.2}Ga_{0.8}As$ act as block layers to prevent external carrier injection from a top electrode and it also make thermally escaped carriers reinject into an optically active layer. A Fe/Au/Ti/Au electrode was deposited on the device surface to apply an electric field. The circularly polarized laser was set to 850 nm for the excitation in GaAs, and the laser power of 5 mW was selected for the efficient PL intensity at RT. A spin-polarized electron and hole pair is generated at GaAs barrier under σ^+-excitation, and then they are injected from the GaNAs QW into the QDs via spin-conserved tunneling, as shown in Fig.6-1(b). In this sample, the electron wave function of GaNAs is penetrated into the QD-ES. Some of spin-polarized electrons

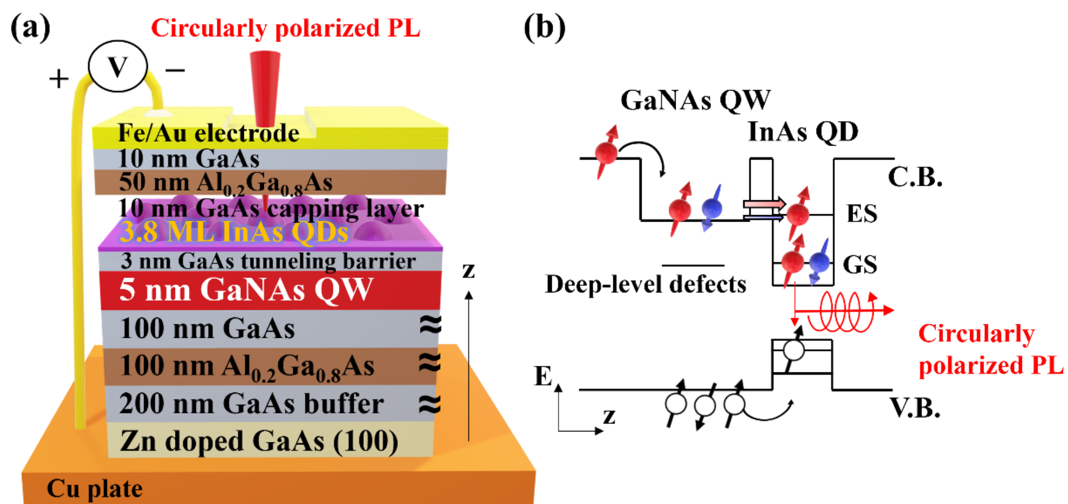

Figure 6-1. Schematic drawings of (a) electric-field-effect optical spin device using GaNAs QW-InAs QD coupled nanostructure and (b) band potentials with a luminescent process reflecting the spin-polarized carrier dynamics in the coupled nanostructure.

can be trapped in deep-level defects formed below the conduction band of GaNAs. The valence band was drawn flat because the sub-band of hole in valence band increases with nitrogen contents [7]. Therefore, spin-polarized holes are injected directly from the GaAs barrier to the QDs.

6.3 Bias dependence of electron-spin polarization at RT

Figure 6-2 shows circularly polarized PL spectra and the corresponding CPD with bias voltages of (a) –2 and (b) 0 V, respectively. The QD-PL intensity peak is observed at 1.01 eV, which corresponds to the PL emission from the QD-GS. The several PL peak above 1.05 eV indicated emissions from the QD-ESs. The PL emissions of the GS and

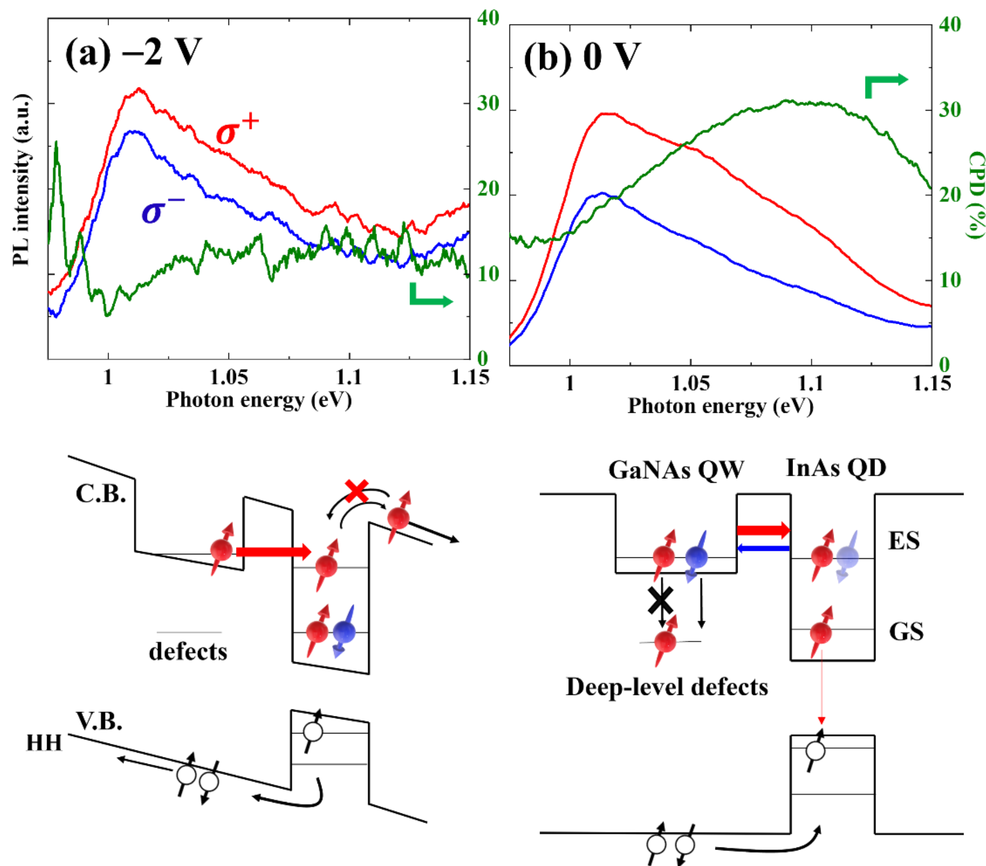

Figure 6-2. Circularly polarized PL spectra and corresponding CPD with bias voltages of (a) –2 and (b) 0 V, respectively. Schematic illustrations of each potential and the possible dynamics of spin-polarized carries are shown below.

ES in the QD ensemble were defined with photon energy ranges of 1 ~ 1.04 eV and 1.06~ 1.11 eV, respectively. At −2 V, PL intensity is rather weak originating from the absence of hole in the QDs owing to the tilted potential of QW-QD coupled structure toward the QD side. In addition, the re-injection of thermally escaped electrons into the QDs is hampered by strong potential modification. The CPD value shows no significant change at both the GS and ES. On the other hand, the CPD changes from 17 % at the QD-GS to 30 % at the QD-ES with a bias voltage of 0 V. This CPD enhancement can be attributed to the remote spin-filtering effect in a GaNAs QW [3]. In the case of 0 V, electrons with majority parallel spin are rapidly trapped by the deep-level defects, and then continuative parallel spin injection into the defects is restricted by Pauli blocking. However, it is possible to inject electrons with minority anti-parallel spin into those defects, therefore only parallel ones are injected into the QDs via spin-conserving tunneling. As a result, parallel PL polarization increases at the QD-ES. At −2 V, the tunneling from the QW to the QD occurs first before spin trapping into the defects due to the potential tilted toward the QDs, therefore spin-filtering effect can be suppressed. In addition, because of the escape of holes from the QDs and the decreased reinjection of thermally escaped electrons into the QDs, PL-CPD values at both the GS and ES decreases.

Bias dependence of the CPD at the QD-GS and ES is shown in Figure 6-3. The CPD at the ES is higher than that at the GS. This result demonstrates the obvious spin-filtering effect by a GaNAs QW. One can guess that the effect of spin filtering is significantly effective at specific bias voltage conditions, such as around 0 V where the potential band becomes flat. Furthermore, it is should be noted that the degree of CPD enhancement depends on the electric field. The CPD value is enhanced two times from 17 % at the QD-GS to 30 % at the ES with a bias voltage

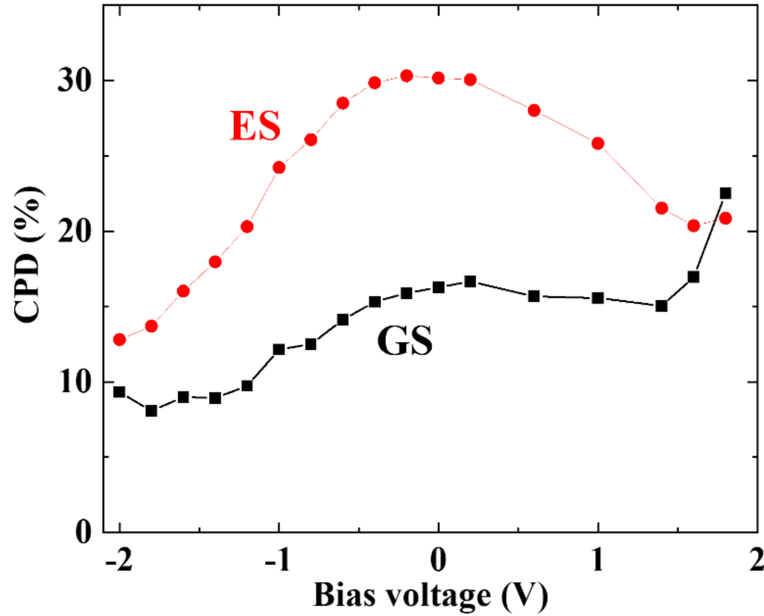

Figure 6-3. Bias dependence of CPD at the QD-GS and ES.

of 0 V. Furthermore, the CPD at the QD-ES is changed from 13 to 30 % by varying bias voltage. This room-temperature voltage control of CPD is corresponding to a 26-60 % change in relative spin polarization, taking the initial spin polarization is 50 % according to the optical selection rule into account. However, the CPD difference between the GS and ES becomes smaller at high and low bias conditions where the potential modification induces the degraded spin filtering effect and the suppressed carrier injection into the QDs.

To elucidate the mechanism of the bias-voltage-dependent amplification effect of the spin-polarized electron at the QD-ES, I performed circularly polarized time-resolved analysis of the QD-PL emission, by varying the bias voltage. Figure 6-4(a) indicates circularly polarized PL time profiles and the corresponding CPD at the QD-ES with −2 and 0 V, respectively. The drastic rise of CPD is observed at 0 V, as compared to that at −2 V. The initial CPD of 20 % increases up to 60 % after 75 ps at 0 V, whereas the maximum CPD of 40 % is obtained at −2 V. This means that the degree of CPD enhancement by the spin filtering

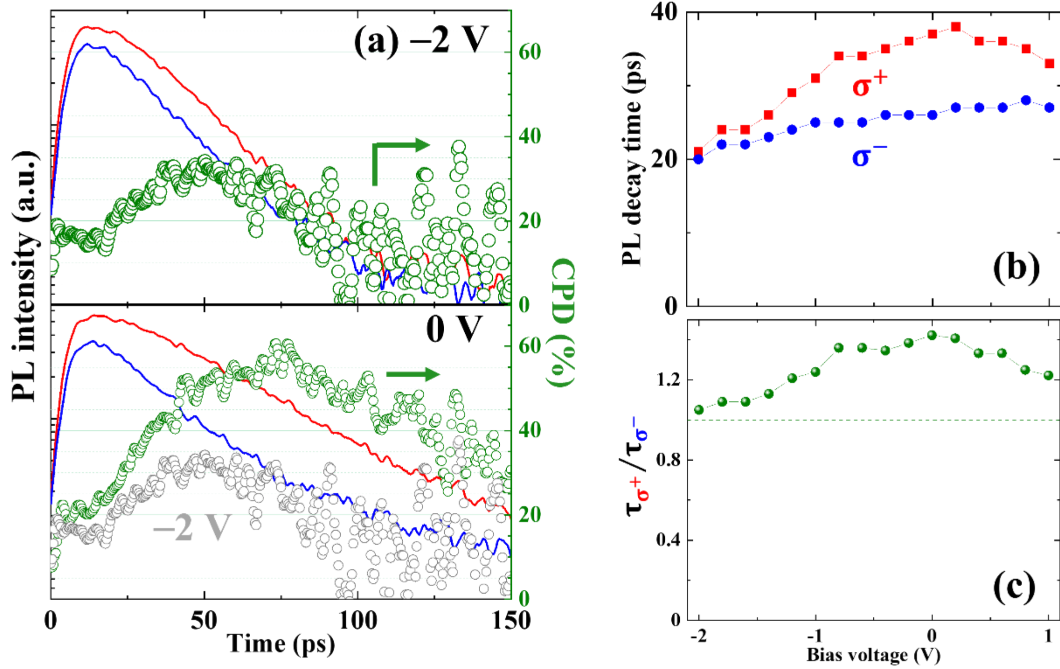

Figure 6-4 (a) Circularly polarized PL time profiles and the corresponding CPD of the QD-GS at -2 and 0 V, respectively. Bias dependences of (c) PL decay time and (c) $\tau_{\sigma^+}/\tau_{\sigma^-}$.

effect depends on bias, as described above. The minority electrons with anti-parallel spin can be trapped directly by deep-level-defects in GaNAs QW via the Pauli blockade after those states are occupied by the majority spins. Therefore, the lifetime of PL emission originating from the minority-spin electrons is shorter than that of majority electrons with parallel spin state within the QD, i.e., $\tau_{\sigma^-} < \tau_{\sigma^+}$ [3]. That is, the difference of PL decay time between the majority and minority spin leads to the CPD amplification, and the number of spin-polarized electrons injected into the QDs is related to the lifetime of PL emission. The degree of CPD amplification is defined as $\tau_{\sigma^+}/\tau_{\sigma^-}$. Here, τ_{σ^+} and τ_{σ^-} denote the decay time of PL including parallel and anti-parallel electron-spins, respectively. The spin filtering effect becomes stronger when $\tau_{\sigma^+}/\tau_{\sigma^-} > 1$. Bias dependences of PL decay time and $\tau_{\sigma^+}/\tau_{\sigma^-}$ at the QD-ES is shown in Fig.6-4 (b) and (c). The degree of CPD amplification is different depending on bias, however, the spin filtering effect is found

at all measured voltages, indicating $\tau_{\sigma^+}/\tau_{\sigma^-} > 1$. High $\tau_{\sigma^+}/\tau_{\sigma^-}$ of 1.4 is obtained around 0 V, and it starts to decrease gradually as increasing or decreasing bias voltages.

Finally, bias dependences of initial and maximum CPD obtained from the time-resolved PL analysis are shown in Figure 6-5. The initial CPD does not notably depends on the bias with values of 12-22 %, but the obvious bias dependence is observed for the maximum CPD. The maximum CPD as a function of bias voltage demonstrates that spin-filtering dynamics strongly relies on electric-field-effect in this GaNAs QW-InAs QD coupled nanostructure. The difference between initial and maximum CPDs is the highest around 0 V, and it exhibits a similar trend as the bias voltage dependence of $\tau_{\sigma^+}/\tau_{\sigma^-}$ ratio, as indicated in Fig.6-4 (c). A decrease in the maximum CPD is related to the decrease of τ_{σ^+} under negative bias conditions. At 0 V, the majority spins are selectively injected into the QDs due to Pauli spin blockade, and thus τ_{σ^+} becomes longer than τ_{σ^-}. On the other hand, τ_{σ^+} is approximately the same as

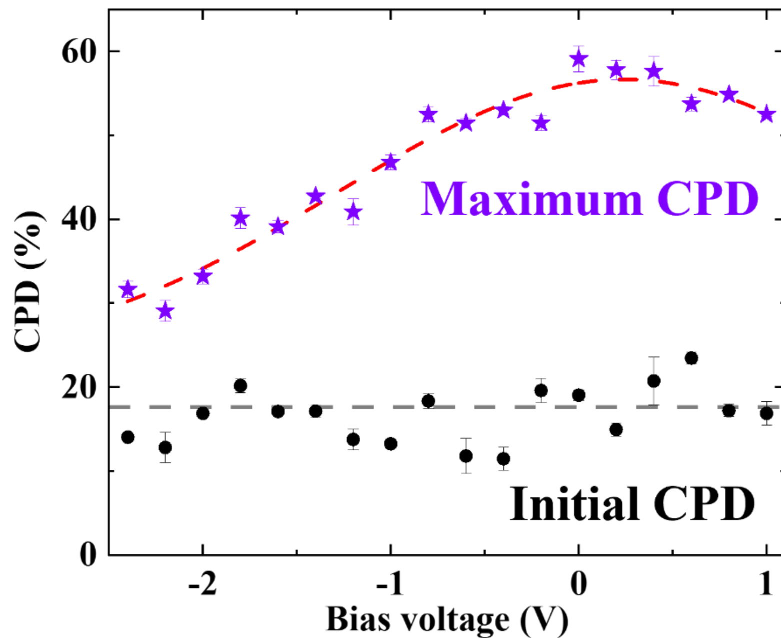

Figure 6-5. Bias dependences of the initial and maximum CPD.

τ_{σ^-} when the number of spin-polarized electrons reinjected into the QDs decreases by the strong potential modification at −2 V. Therefore, the maximum CPD decreases to down 30 % owing to thermal escape of spin-polarized electrons from the QDs.

6.4 Conclusion

I have studied the bias dependences of the PL-CPD reflecting electron-spin polarization in the electric-field-effect optical spin devices using GaNAs QW-InAs QD tunnel-coupled nanostructures newly developed. The remote spin-filtering effect within the GaNAs QW induces the CPD increase owing to amplification of the electron-spin polarization at the QD-ES as well as QD-ES. The room-temperature voltage control of CPD obtained at the QD-ES is corresponding to a 26-60 % change in relative spin polarization. I find that the degree of CPD amplification strongly depends on external electric field, and the electric-field-induced potential modification degrades spin-filtering-effect. The maximum value of CPD up to 60 % is obtained around 0 V.

Bibliography

[1] N. -T. Yeh, T. -E. Nee, and J. -I. Chyi, Appl. Phys. Lett. **76**, 1567 (2000).

[2] X. Q. Zhang, S. Ganapathy, H. Kumano, K. Uesugi, and I. Suemune, J. Appl. Phys. **92**, 6813 (2002).

[3] Y. Huang, V. Polojarvi, S. Hiura, P. Hojer, A. Aho, R. Isoaho, T. Hakkarainen, M. Guina, S. Sato, J. Takayama, A. Murayama, I. A. Buyanova, and W. M. Chen, Nat. Photonics **15**, 475 (2021).

[4] X. J. Wang, I. A. Buyanova, F. Zhao, D. Lagarde, A. Balocchi, X. Marie, C. W. Tu, J. C. Harmand, and W. M. Chen, Nat. mater. **8**, 198 (2009).

[5] Y. Puttisong, I. A. Buyanova, L. Geelhaar, H. Riechert, C. W. Tu, and W. M. Chen, J. Appl. Phys. **111**, 07C303 (2012).

[6] Y. Puttisong, I. A. Buyanova, A. J. Ptak, C. W. Tu, L. Geelhaar, H. Riechert, and W. M. Chen, Adv. Mater. **25**, 738 (2013).

[7] J. Shao, W. Lu, and M. Sadeghi, X. Lu, S. M. Wang, L. Ma, and A. Larsson, Appl. Phys. Lett. **93**, 031904 (2008).

Chapter 7. Conclusion

I fabricated electric-field-effect optical spin devices using QW/QD tunnel-coupled nanostructures and investigated the temperature dependences of the electron-spin polarization and the resultant PL circular polarization property.

1. I have studied an electric-field effect on the degree of the circular polarization degree (CPD) reflecting electron-spin polarization as a function of temperature, using InGaAs QW-QD tunnel-coupled nanostructures. The CPD changes in the range of 3-15 % at room temperature (RT) by an external bias application, corresponding to a 12-60 % change in the internal electron-spin polarization P_{rel}^{QD} in the QDs after spin injection from the QW. Despite RT, I find to control the CPD by using an external electric field only. In addition, the spin-flip dynamics within the QDs is observed even at RT, and it can be also controlled by the electric field. This can greatly facilitate the practical applications of optically functional semiconductor spintronics by means of electric-field manipulation, which is one the most traditional and effective techniques of the modern electronics.

2. I studied the temperature dependence of the PL-CPD reflecting the spin polarization in electric-field-effect optical spin devices using InGaAs QW-InAs QD coupled nanostructures instead of employing InGaAs QDs. A significant energy-dependent oscillation of the PL intensity is observed at low temperatures, originating from LO-phonon mediated resonant tunneling between the ground state (GS) of QW and QD excited states (ESs). This can promote efficient, i.e., ultrafast and spin-conserved, injection of spin-polarized electrons from the QW as a spin reservoir into the QDs as an optically active medium. The negative PL polarization, which indicates anti-parallel spins in the QDs against for

those initially excited in the QW, disappears at 160 K, suggesting the thermal escape of residual electrons with parallel spin polarization from the GS of the InAs QD.

3. I have studied the electron-spin polarization and the resultant PL circular polarization in electric-field-effect optical spin devices using GaNAs QW-InAs QD coupled nanostructures newly developed. The remote spin-filtering effect within the GaNAs QW can induce significant amplification of the electron-spin polarization, i.e., the CPD value of the PL, at the QD-GS as well as QD-ES. I find that the value of CPD can be significantly enhanced at RT, owing to the spin amplification in the GaNAs before the spin injection, and also strongly depends on a strength of external electric field.

   As a result, I have achieved electric-field control of the electron-spin polarization and the resultant circular polarization in the InAs QDs after the spin injection from the GaNAs QW, even at RT, in the range of 10 %, i.e., 13-30 % of the PL-CPD at the QD-ES with the bias application from −1.5 to 1.5 V. This room-temperature voltage control of CPD is corresponding to a 26-60 % change in relative spin polarization, because the initial spin polarization excited on GaAs barriers is 50 % according to the optical selection rule.

Research achievements

Publications

1. Hang Chen, Satoshi Hiura, Junichi Takayama, Soyoung Park, Kazuhisa Sueoka, and Akihiro Murayama, “Electric field control of spin polarity in spin injection into InGaAs quantum dots from a tunnel-coupled quantum well”, Appl. Phys. Lett. **114**, 133101 (2019).

2. Hang Chen, Satoshi Hiura, Junichi Takayama, Soyoung Park, Kazuhisa Sueoka, and Akihiro Murayama, “Enhanced hetero-dimensional electron-spin injection in a resonantly tunnel-coupled InGaAs quantum dot-well nanosystem”, Appl. Phys. Express **13**, 015003 (2020).

3. Soyoung Park, Hang Chen, Satoshi Hiura, Junichi Takayama, Kazuhisa Sueoka, and Akihiro Murayama, “Electric-filed-effect spin switching with an enhanced number of highly polarized electron and photon spins using p-doped semiconductor quantum dots”, ACS Omega **6**, 12, 8561 (2021).

4. Kohei Etou, Satoshi Hiura, Soyoung Park, Kazuya Sakamoto, Junichi Takayama, Agus Subagyo, Kazuhisa Sueoka, and Akihiro Murayama, “Room-temperature spin-transport properties in an $In_{0.5}Ga_{0.5}As$ quantum dot spin-polarized light-emitting diode”, Phys. Rev. Appl. **16**, 014034 (2021).

5. Mai Ugajin, Soyoung Park, Takayuki Kiba, Junichi Takayama, Satoshi Hiura, Akihiro Murayama, Midori Kawamura, and Yoshio Abe, “Optical characterization and emission enhancement property of Ag nanomesh structure fabricated by nanosphere lithography”, Surface & Coatings Technology **435**, 128258 (2022).

6. Soyoung Park, Satoshi Hiura, Junichi Takayama, Kazuhisa Sueoka, and Akihiro Murayama, “Efficient room-temperature voltage control of picosecond optical spin orientation using a III-V semiconductor nanostructures”, Adv. Electron. Mater. **8**, 2200588 (2022).

Conferences

International conference

1. "Electric-field control of optical-spin injection from an InGaAs quantum well to *p*-doped quantum dots",
   ○Soyoung Park, Hang Chen, Junichi Takayama, Satoshi Hiura, and Akihiro Murayama, Compound Semiconductor Week 2019, May 19-23, 2019 (refereed poster).

2. "Electric-field-effect optical spin-injection device using *p*-doped InGaAs quantum dots",
   ○Soyoung Park, Hang Chen, Junichi Takayama, Satoshi Hiura, and Akihiro Murayama, Semicon Nano 2019, Sep 24-27, 2019 (refereed poster).
   *Best poster award

3. "Electron-spin dynamics in tunnel-coupled structures of InGaAs well and dot with different p-doping concentrations applied with electric field",
   ○Soyoung Park, Hang Chen, Satoshi Hiura, Junichi Takayama, and Akihiro Murayama, Solid State Devices and Materials 2020, Sep. 27~30, 2020, H-4-02 (Oral).

4. "Electric-Field Control of Electron-Spin Polarization Degree at Room Temperature in Opto-Spintronic Device Using InGaAs Quantum Dots",
   ○Soyoung Park, Satoshi Hiura, Hang Chen, Junichi Takayama, Kazuhisa Sueoka, and Akihiro Murayama, Solid State Devices and Materials 2021, Sep. 6~9, 2021, I-1-06 (Oral).

5. "Optical Spin Properties of InAs Quantum Dots Tunnel-Coupled with Dilute Nitride GaNAs",
   ○Shino Sato, Yuto Nakamura, Soyoung Park, Satoshi Hiura, Junichi Takayama, and Akihiro Murayama, Solid State Devices and Materials 2021, Sep. 6~9, 2021, H-4-04 (Oral).

6. "Temperature Effects on Performances of a Spin-Polarized Light Emitting Diode using p-Doped InGaAs Quantum Dots",
   ○Kohei Eto, Satoshi Hiura, Junichi Takayama, Soyoung Park, Agus Subagyo, Kazuhisa Sueoka, and Akihiro Murayama, Solid State Devices and Materials 2021, Sep. 6~9, 2021, E-5-03 (Oral).

7. "Bias voltage and temperature dependence of electron-spin polarization in InAs quantum dots tunnel-coupled with a GaNAs quantum well",
   Soyoung Park, ○Hiroto Kise, Satoshi Hiura, Junichi Takayama, Kazuhisa Sueoka, and Akihiro Murayama, Solid State Devices and Materials 2022, Sep. 23~25, 2022,

Domestic conference

1. "Electric-field control of electron spin injection into p-doped quantum dots",
   ○Soyoung Park, Hang Chen, Satoshi Hiura, Junichi Takayama, and Akihiro Murayama,
   The 80nd JSAP Autumn Meeting 2019, Sep. 18~21, 2019, 18p-E216-10 (Oral).

2. "p-doping concentration dependence of electron-spin dynamics in InGaAs quantum well-dot coupled structures applied with electric field",
   ○Soyoung Park, Hang Chen, Satoshi Hiura, Junichi Takayama, and Akihiro Murayama,
   The 81st JSAP Autumn Meeting 2020, Sep. 8~11, 2020, 8p-Z08-7 (Oral).

3. "Temperature dependence of electron-spin polarization in InGaAs quantum dot opto-spintronic device applied with electric field",
   ○Soyoung Park, Satoshi Hiura, Hang Chen, Junichi Takayama, Kazuhisa Sueoka, and Akihiro Murayama,
   The 82nd JSAP Autumn Meeting 2021, Sep. 10~13, 2021, 12p-S302-1 (Oral).
   *English session award

4. "Temperature dependence of circular polarization properties of electroluminescence in quantum dot spin-polarized light-emitting diode",
   ○Kohei Eto, Satoshi Hiura, Soyoung Park, Junichi Takayama, Agus Subagyo, Kazuhisa Sueoka, and Akihiro Murayama,
   The 82nd JSAP Autumn Meeting 2021, Sep. 10~13, 2021, 10p-N303-12.

5. "Spin dynamics in tunnel-coupled structure of dilute nitride GaAs and InAs quantum dots",
   ○Shino Sato, Yuto Nakamura, Soyoung Park, Satoshi Hiura, Junichi Takayama, and Akihiro Murayama,
   The 82nd JSAP Autumn Meeting 2021, Sep. 10~13, 2021, 12p-N303-6.

6. "Emission Enhancement of Organic Emitter with Ag Nanomesh Structure",
   ○Mai Ugajin, Soyoung Park, Takayuki Kiba, Midori Kawamura, Yoshio Abe, Junichi Takayama, Satoshi Hiura, and Akihiro Murayama,
   The 82nd JSAP Autumn Meeting 2021, Sep. 10~13, 2021, 12p-N207-3.

7. "Bias dependence of electron-spin polarization in GaNAs quantum well-InAs quantum dot tunnel-coupled structures",
   ○Hiroto Kise, Soyoung Park, Satoshi Hiura, Junichi Takayama, Kazuhisa Sueoka, and Akihiro Murayama,
   The 83rd JSAP Autumn Meeting 2022, Sep. 20~23, 2022, 23p-B201-12.

8. "Circularly polarized electroluminescence properties of quantum dot spin-polarized light-emitting diodes using GaNAs spin filter",
   ○Kohei Eto, Satoshi Hiura, Soyoung Park, Junichi Takayama, Agus Subagyo, Kazuhisa Sueoka, and Akihiro Murayama,
   The 83rd JSAP Autumn Meeting 2022, Sep. 20~23, 2022, 23a-B201-5.